OXFORD

ORIGINAL ARTICLE

Loss of Either Rac1 or Rac3 GTPase Differentially Affects the Behavior of Mutant Mice and the Development of Functional GABAergic Networks

Roberta Pennucci[1,†], Francesca Talpo[3,†], Veronica Astro[1],
Valentina Montinaro[1], Lorenzo Morè[4], Marco Cursi[2], Valerio Castoldi[2],
Sara Chiaretti[1], Veronica Bianchi[4], Silvia Marenna[2], Marco Cambiaghi[2],
Diletta Tonoli[1], Letizia Leocani[2], Gerardo Biella[3], Patrizia D'Adamo[4] and
Ivan de Curtis[1]

[1]Cell Adhesion Unit, Division of Neuroscience, [2]Experimental Neurophysiology Unit, INSPE-Institute of
Experimental Neurology, Division of Neuroscience, IRCSS San Raffaele Scientific Institute and San Raffaele
University, Milano 20132, Italy, [3]Department of Biology and Biotechnology "L. Spallanzani", University of Pavia,
Italy and [4]Molecular Genetics of Mental Retardation Unit, Division of Neuroscience, IRCSS San Raffaele Scientific
Institute, Milano, Italy

Address correspondence to Ivan de Curtis, Division of Neuroscience, San Raffaele Scientific Institute and San Raffaele University, Via Olgettina 58,
20132 Milano, Italy. Email: decurtis.ivan@hsr.it

[†]These authors contributed equally to this study.

Abstract

Rac GTPases regulate the development of cortical/hippocampal GABAergic interneurons by affecting the early development and
migration of GABAergic precursors. We have addressed the function of Rac1 and Rac3 proteins during the late maturation of
hippocampal interneurons. We observed specific phenotypic differences between conditional Rac1 and full Rac3 knockout mice.
Rac1 deletion caused greater generalized hyperactivity and cognitive impairment compared with Rac3 deletion. This phenotype
matched with a more evident functional impairment of the inhibitory circuits in Rac1 mutants, showing higher excitability and
reduced spontaneous inhibitory currents in the CA hippocampal pyramidal neurons. Morphological analysis confirmed a
differential modification of the inhibitory circuits: deletion of either Rac caused a similar reduction of parvalbumin-positive
inhibitory terminals in the pyramidal layer. Intriguingly, cannabinoid receptor-1-positive terminals were strongly increased only in
the CA1 of Rac1-depleted mice. This increase may underlie the stronger electrophysiological defects in this mutant. Accordingly,
incubation with an antagonist for cannabinoid receptors partially rescued the reduction of spontaneous inhibitory currents in the
pyramidal cells of Rac1 mutants. Our results show that Rac1 and Rac3 have independent roles in the formation of GABAergic
circuits, as highlighted by the differential effects of their deletion on the late maturation of specific populations of interneurons.

Key words: CB1R, hyperactivity, inhibitory synapses, neuronal maturation, VGAT

Introduction

Inhibitory γ-aminobutyric acid (GABA)ergic interneurons are fundamental players in modulating the activity of the neuronal circuits (Batista-Brito and Fishell 2009; Gelman and Marín 2010). The abnormal maturation of cortical and hippocampal interneurons is believed to alter the balance between excitatory and inhibitory activity in the brain, and to cause neural and intellectual disabilities as those observed in epilepsy, autism, and schizophrenia (Brooks-Kayal 2011). The majority of the cortical and hippocampal GABAergic interneurons are born in the ventral telencephalon, migrating from either the caudal or medial ganglionic eminences (CGE and MGE, respectively) (Wonders and Anderson 2006). These GABAergic interneurons distribute throughout the cortex and hippocampus where they establish synaptic contacts with excitatory pyramidal neurons or other interneurons (Morozov et al. 2006).

Several extracellular cues have been shown to drive the migration and differentiation of the cortical and hippocampal GABAergic cells, while very little is known about the intracellular mechanisms that drive the different phases of their maturation (Hernández-Miranda et al. 2010). Rac proteins are members of the family of Rho GTPases with important regulatory functions on the cytoskeleton, and critical in several aspects of neuronal development (de Curtis 2008). Vertebrates express 2 Rac proteins in their brain, Rac1 and the neural-specific, developmentally regulated Rac1B/Rac3 (Malosio et al. 1997; Bolis et al. 2003; Corbetta et al. 2005). Recent studies have used mouse genetics to address the function of the 2 Rac proteins in the development of cortical and hippocampal interneurons (Chen et al. 2007; Vidaki et al. 2012; Vaghi et al. 2014; Tivodar et al. 2015). We have shown that the deletion of both proteins affects the migration of postmitotic interneurons, leading to the impairment of the brain circuitry and the early onset of spontaneous epileptic seizures (Vaghi et al. 2014). These phenotypes correspond to a defect in the development of specific neuronal populations. The number of Lhx6-positive cortical and hippocampal interneurons originating in the MGE was reduced. This finding matches with a drastic decrease of the number of parvalbumin (PV)-positive cells, largely deriving from precursors born in the MGE (Tricoire et al. 2011; Inan et al. 2012). The severity of this defect was dependent on the combined loss of Rac1 and Rac3, although we could observe milder but significant decreases in the number of PV-positive cells also in the developing brain of single Rac1N or Rac3KO mice. Therefore, while the loss of one Rac protein may be compensated by the other in the development of this class of interneurons, each GTPase also performs specific functions. Here, we have addressed the effects of single Rac deletion on the maturation of the cortical–hippocampal interneuronal network, with the aim of identifying specific functions for the 2 GTPases. We found that Rac1 and Rac3 contribute differently to the development of hippocampal PV-positive GABAergic interneurons. Deletion of either Rac leads to a similar moderate loss of PV-positive interneurons, but affects differently the morpho-functional development of the hippocampal circuits. These dissimilarities may underlie the distinct behavioral and neurological consequences observed in Rac1N and Rac3KO mice. The analysis of single Rac deletion during late neuronal maturation highlights specific morphological and functional phenotypes that are not compensated by the remaining Rac.

Materials and Methods

Mice

Experimental handling of mice was approved by the National Ministry of Health, in accordance with institutional guidelines and EEC regulation 86/609/CEE. Transgenic lines used in this study, including Rac3KO mice, and conditional KO mice for Rac1 (Rac1N) obtained by crossing Rac1flox/flox Walmsley et al. 2003) with Synapsin-I-Cre (Syn-Cre) mice (Zhu et al. 2001) to delete Rac1 in postmitotic developing neurons, have been characterized previously (Corbetta et al. 2005, 2009). In the experiments, controls for Rac3KO and Rac1N mice were wild-type (WT), and Rac1flox/flox or Rac1flox/+ (Rac1flox) littermates, respectively. The genotypes were determined as described (Corbetta et al. 2009).

Antibodies

Antibodies included rabbit polyclonal anti-PV, 1:2000, PV-28 from Swant; goat polyclonal anti-PV, 1:300, PVG-214 from Swant; rabbit polyclonal anti-vesicular GABA transporter (VGAT), 1:150, from Synaptic Systems; mouse monoclonal anti-Rac1 (BD Transduction); anti-glutamic acid decarboxylase 67 (GAD67), 1:100, from Chemicon International; mouse monoclonal anti-tubulin-α, anti-synapsin-I (clone G143) and anti-GAD65 antibody, 1:250, clone GAD-6 from Sigma; the affinity-purified rabbit anti-cannabinoid 1 receptor (CB1R) CB1-L15, 1:250, was a kind gift from Ken Mackie (Indiana University, Bloomington, IN). Alexa Fluor-conjugated secondary antibodies (1:200, from Invitrogen); biotinylated goat anti-rabbit antibodies (1:200, from Vector Laboratories).

Biochemistry

Immunoblotting with anti-Rac1 and anti-tubulin antibodies were performed on lysates from adult brain prepared as described (Corbetta et al. 2009).

Morphological Analysis and Quantification

Mice subjected to anesthesia were perfused with 4% paraformaldehyde, and brains postfixed with 4% paraformaldehyde and cryoprotected before freezing. Twelve micrometer thick sections were incubated overnight at 4°C with primary antibodies detected then with a Vectastain Elite ABC Kit (Vector Laboratories). Sections were viewed with a Zeiss Axioplan2 microscope with AxioCam MRc5 digital camera (Carl Zeiss MicroImaging). For immunofluorescence, primary antibodies were incubated for 12–72 h at 4°C and revealed by 1.5 h incubation with Alexa Fluor-conjugated secondary antibodies and 4′,6-diamidino-2-phenylindole (DAPI, Sigma-Aldrich) for nuclear staining. Sections were viewed with a Zeiss Axiovert 135 TV equipped with a QImaging Exi-Blue camera (Carl Zeiss MicroImaging). Confocal analysis was performed with a Leica TCS SP2 microscope (Leica Microsystems).

For each genotype, 3–8 sections along the rostro-caudal axis of the dorsal hippocampus of 3–5 sets of littermates were used for quantifications. The density of PV-positive cells was evaluated from similar areas of the hippocampus using the ImageJ software (NIH).

The areas occupied by the fluorescent signals for PV, VGAT, GAD67, or CB1R were evaluated from coronal sections including comparable levels of either the CA1 or the CA3 pyramidal layer. Quantification of the area occupied by the markers was performed on equal areas of the pyramidal layer (=total area) from the different genotypes. Values were expressed as the percentage of the corresponding total area, from which the area occupied by the nuclei was excluded. Pinhole was kept constant at one Airy unit, laser power, and photomultiplier settings were the same for all samples within the same experiment. Quantitative

analysis of the localization or colocalization of PV, VGAT, GAD67, and CB1R was performed using ImageJ, and normalized to the respective controls (=100%). All graphs show means ± SEM. Statistical significance was determined by the Student's *t*-test.

The quantification of the presynaptic terminals positive for CB1R or PV and VGAT was performed using the "Analyze Particles" function of ImageJ on thresholded confocal images. The same threshold was applied on equal areas of the pyramidal layer for sections of the different genotypes. For each selected area, the density of terminals was calculated by dividing the number of positive dots by the number of DAPI-positive nuclei. The normalized terminal density represents the mean value of different areas from 3 mice per genotype that was normalized to the respective control (=100%).

For 5-bromo-4-chloro-3-indolyl-β-D-galactopyranoside (X-Gal) staining, Syn-Cre mice were mated with LacZ ROSA26 tester reporter mice (Soriano 1999). The brain from adult mice was fixed and used for X-Gal staining and immunohistochemistry for PV as described (Vaghi et al. 2014).

Behavioral Analysis

Animals were maintained on a reversed 12 h light/darkness cycle at 22–24°C. Food and water were available ad libitum in the home cage. All behavioral procedures were approved by the Animal Care of the San Raffaele Scientific Institute, and by the National Ministry of Health (IACUC #653). All the behavioral tests were assessed on 3 to 4-months-old mice, comparing WT with Rac3KO littermates, and Rac1N with Rac1flox littermates. Additionally, to exclude effects of the Syn-Cre transgene on behavioral performance, Rac1flox mice were compared with Syn-Cre and WT (C57Bl6/N) mice in the emergence and spontaneous alternation tests.

Dark–light box, emergence and novelty tests were used to assess explorative and emotional behavior (for detailed test procedure see Madani et al. 2003). The hidden-platform version of the water maze was used to test spatial reference memory (Wolfer and Lipp 1992). Visual ability was tested in the flag-visible version for 4 consecutive trials in one day. Spontaneous alternation task was used to measure hippocampus-dependent spatial working memory in a nonfood rewarded (D'Adamo et al. 2014) task. A mouse was released in the central hub of a cross maze (4 arms) and left free to explore for 10 min. Number and sequence of arm entries were recorded. A correct alternation was considered when no more than one repetition over 5 entries was made. Spatial working memory was tested in food rewarded 8-arm radial maze as previously described (D'Adamo et al. 2002). Trace fear conditioning was used to test hippocampal-dependent associative memory as previously described (D'Adamo et al. 2002). Briefly, during the training phase the delivery of the unconditioned stimulus (US: foot shock) was delivered at the end of the presentation of the conditioned stimulus (CS: tone), with a CS–US interval of 15 s. Twenty-four hours after conditioning, context memory (CTX) and CS memory (CUE) were tested. CTX took place in the training chamber and consisted of 2-min observation. CUE memory took place in a different chamber and consisted of 1-min without (Bl: baseline) followed by 1-min with the CS turned on (CUE).

During all tests, animals were video-tracked using the EthoVision 2.3 system (Noldus Information Technology, Wageningen, Netherlands), with an image frequency of 4.2/s. Raw data were transferred to Wintrack 2.4 for off-line analysis. Analysis of variance (ANOVA) with repeated measures was used for statistical analysis (SAS Institute, Cary, NC, USA). Normal distribution and

homogeneity of variances among our data samples were tested with the K–S normality test and Bartlett's test for homogeneity. Our data did not differ significantly from computed ideal variables. Main effects were verified using nonparametric tests.

Electrophysiology

Electrophysiological experiments were performed on hippocampal slices prepared from 3 to 6-weeks-old WT, Rac1flox, Syn-Cre, Rac1N, and Rac3KO mice. Animals were anesthetized by inhalation of isoflurane and transcardially perfused with cold (<4°C), carboxygenated (95% O_2, 5% CO_2) cutting solution (70 mM sucrose, 80 mM NaCl, 2.5 mM KCl, 26 mM $NaHCO_3$, 15 mM glucose, 7 mM $MgCl_2$, 1 mM $CaCl_2$, 1.25 mM NaH_2PO_4). Transversal 350-μm-thick slices (Stoop and Pralong 2000) were transferred to an incubation chamber filled with carboxygenated aCSF medium (125 mM NaCl, 2.5 mM KCl, 26 mM $NaHCO_3$, 15 mM glucose, 1.3 mM $MgCl_2$, 2.3 mM $CaCl_2$, 1.25 mM NaH_2PO_4). All recordings were performed at 23–25°C on submerged slices perfused at 0.6 mL/min with aCSF. The recording chamber was mounted on an E600FN microscope equipped with a 4× lens and a 40× water-immersion objective (Nikon), and connected to a near-infrared CCD camera. The data were derived from CA3 and CA1 pyramidal neurons using the whole-cell patch-clamp technique in voltage- and current-clamp mode. To investigate the susceptibility to induce ictal-like epileptiform activity, the following intracellular solution was used: 130 mM K-gluconate, 4 mM NaCl, 2 mM $MgCl_2$, 1 mM EGTA, 5 mM creatine phosphate, 2 mM Na_2ATP, 0.3 mM Na_3GTP, 10 mM HEPES (pH 7.3 with KOH). To register the inhibitory chloride-mediated GABAergic postsynaptic currents (IPSCs), pipettes were filled with 120 mM Cs-methanesulphonate, 5 mM KCl, 1 mM $CaCl_2$, 2 mM $MgCl_2$, 10 mM EGTA, 4 mM Na_2ATP, 0.3 mM Na_3GTP, 5 mM lidocaine N-ethylbromide, 8 mM HEPES (pH 7.3 with KOH). Membrane voltage was corrected off-line for a measured liquid junction potential. Series resistance was always compensated by 70–90% and monitored throughout the experiment. Recordings were made with a MultiClamp 700B amplifier (Molecular Devices) and digitized with a Digidata 1322 computer interface (Molecular Devices). Data were acquired using the software Clampex 9.2 (Molecular Device), sampled at 20 kHz and filtered at 10 kHz.

All drugs were added to the aCFS medium. The induction of epileptiform-like discharges was performed by perfusion with 500 μM 4-aminopyridine (4-AP, Sigma-Aldrich), a selective blocker of the A-type potassium channels.

The IPSCs recordings were carried out in the presence of glutamatergic synaptic blockers: 10 μM 2,3-Dioxo-6-nitro-1,2,3,4-tetrahydrobenzo[*f*]quinoxaline-7-sulfonamide (NBQX, Tocris Cookson), an AMPA receptor antagonist, and 30 μM 3-(2-carboxypiperazin-4-yl)propyl-1-phosphonic acid (CPP, Tocris Cookson), an NMDA receptor antagonist. IPSCs were abolished by 10 μM bicuculline methiodide (bicuculline, Sigma-Aldrich), a $GABA_A$ receptor antagonist. N-piperidino-5-(4-chlorophenyl)-1-(2,4-dichlorophenyl)-4-methyl-3-pyrazolecarboxamide HCL (SR141716A, Sigma-Aldrich) was used diluted to 1 μM in aCFS supplemented with 1 g/L BSA to antagonize the CB1Rs.

Data were analyzed with the software Clampfit 10.2 (Molecular Devices) and Origin (Microcal). Cell surface was estimated by integrating the capacitive current evoked by a −10 mV pulse. Neuronal input resistance (R_{in}) was calculated in the linear portion of the *I*–*V* relationship during depolarizing voltage responses near the resting potential. To analyze the 4-AP-induced seizure-like activity, the preictal events, the ictal discharge, and the afterdischarge were detected and characterized. For the

analysis presented in this study, synchronous epileptiform events shorter than 3 s that generally precede the ictal-like discharge are indicated as "preictal activity", while sustained events are termed "ictal-like activity"; highly synchronous events that may occur after the ictal-like activity are indicated as afterdischarges.

The IPSCs were detected manually: the amplitude of the events obeyed a log-normal distribution and accordingly the mean amplitudes were computed using a log-normal function; the interevent intervals were distributed exponentially, and mean frequencies were obtained from the best monoexponential fit of each distribution. All measurements are presented as means ± SEM. Statistical significance was determined by the Student's t-test and by one-way ANOVA.

Video-EEG Recording and Analysis

WT ($n = 12$), Syn-Cre ($n = 12$), Rac1flox ($n = 20$), Rac1N ($n = 20$) and Rac3KO ($n = 20$) mice underwent video-electroencephalogram (EEG) recording, as already described (Cambiaghi et al. 2013). Briefly, epidural screw electrodes were implanted under sevoflurane anesthesia (Sevorane™, Abbott S.p.a. Campoverde, Italy). Two electrodes were placed on the right and left parietal areas and one over cerebellum as a common reference. After 3 days, mice were monitored by video-EEG for 6–48 h. Data were digitally recorded with a System Plus device (Micromed, Mogliano Veneto, Italy). EEG traces were filtered between 0.53 and 60 Hz, sampled at 256 Hz and coded with 12 bits. Four animals per genotype were recorded for each age group, each one consisting of 20 consecutive days, between postnatal day 20 (P20) and P120. Video-EEG recordings were visually inspected to detect spontaneous seizures, defined as high-amplitude (at least 2 times the baseline) rhythmic discharges lasting at least 5 s.

Power spectra of the background EEG activity were calculated by Fast Fourier Transform (FFT) using the Welch periodogram method (Welch 1967). The analysis was performed during the awake state recognized by video recording inspection. For each recording, 3–4 min of artefact-free traces were selected for spectral analysis, at least 1 h after the start of recording. EEG sessions including spontaneous seizures at any time were not considered. FFT was applied on epochs of 2 s within the selected period, tapered with a Hanning window, obtaining a spectrum for each epoch with a frequency resolution of 0.5 Hz. The mean power spectrum was then estimated by averaging the single epoch spectra and the 2 channels. Absolute power values were then normalized to the total absolute power to obtain relative values comparable among the different animals. Spectral analyses were performed using the EEG Analyzer function included in the software Micromed System PLUS.

The mean dominant frequency (MDF), defined as the "center of mass" of a frequency band, was calculated from power spectra within delta (1–4 Hz), and theta–alpha (6–10 Hz) bands, as the weighted mean of the frequencies included within the band, with their corresponding power values as weight. (Cambiaghi et al. 2013). Statistical analysis was performed using one-way ANOVA on delta and theta–alpha relative power and MDF values, considering the factor GROUP (WT, Syn-Cre, Rac1flox, Rac1N and Rac3KO) and using the Bonferroni post hoc analysis.

Results

Rac1N Mice Show Generalized Hyperactivity

We previously found that Rac3 KO mice show hyperactivity not associated with anxiety or curiosity, but to higher generalized basal activity (Corbetta et al. 2008). Here we evaluated Rac1N mice in the dark/light, emergence and novelty tests to assess explorative and anxiety-like behavior and to look for behavioral differences between Rac3KO and Rac1N mice. Like Rac3KO, Rac1N mice did not show anxiety-like behavior in the dark/light box, as displayed by the significantly longer time spent outside the dark compartment (genotype effect, $F_{1,23} = 7.13$, $P = 0.014$, Fig. 1A). Moreover, the analysis of their locomotor activity showed no differences between genotype for the traveled distance (genotype effect, $F_{1,23} = 2$, $P = 0.17$, Fig. 1B) and speed (genotype effect, $F_{1,22} = 0.32$, $P = 0.57$, data not shown).

In the emergence test, a significant difference was observed in Rac1N mice compared with all control mice (Rac1flox, Syn-Cre, and WT mice) in the time spent inside the box (genotype effect, $F_{1,24} = 24.25$, $P < 0.0001$, Fig. 1C and Supplementary Fig. 1A), but the duration of invisible periods between genotypes was similar (genotype effect, $F_{1,24} = 1.4$, $P = 0.24$, Supplementary Fig. 1B), possibly caused by an increase of locomotor activity rather than anxiety-like behavior. This hypothesis is supported by the finding that Rac1N mice showed increased locomotor activity (genotype effect, $F_{1,24} = 47.9$, $P < 0.0001$, Fig. 1D) and speed (genotype effect, $F_{1,24} = 25.7$, $P < 0.0001$, data not shown), especially in the home zone close to the familiar box (Supplementary Fig. 1C, blue dots), with a significant increase in the number of excursions (genotype effect, $F_{1,24} = 72.6$, $P < 0.0001$, Supplementary Fig. 1D).

In the novel object test, Rac1N mice spent significantly less time in the safe zone (genotype effect, $F_{1,24} = 22.36$, $P < 0.0001$, Fig. 1E). As for the emergence test, Rac1N showed a highly significant increase in the total distance traveled in both sessions of the test (genotype effect, $F_{1,24} = 25.94$, $P = 0.0002$, Fig. 1F and Supplementary Fig. 1E) and in the speed (genotype effect, $F_{1,24} = 15.7$, $P = 0.0006$, data not shown). The introduction of the novel object into the center of the arena during the second part (30 min) of the test induced the Rac1N mice to approach and investigate more the object than their control littermates (genotype effect, $F_{1,24} = 26.6$, $P = 0.0006$, Fig. 1G and Supplementary Fig. 1E). These results indicate that Rac1N mice have a greater generalized hyperactivity when compared with Rac3 KO mice, previously tested under identical conditions (Corbetta et al. 2008).

Phobia in Rac1N Mice Impairs Spatial Reference Memory

The water maze was used to test hippocampal-dependent spatial learning and memory that we have previously shown to be unaffected in Rac3KO mice (Corbetta et al. 2008). Instead, Rac1N mice were significantly different from control mice in the wall hugging (genotype effect, $F_{1,22} = 39.9$, $P < 0.0001$, Fig. 2A) and floating time (genotype effect, $F_{1,22} = 44.6$, $P < 0.0001$, not shown), particularly in the first 8 trials of the acquisition phase. The swim speed was significantly decreased in Rac1N mice (genotype effect, $F_{1,22} = 109.7$, $P < 0.0001$, Fig. 2B). These defects suggest a possible increase in either anxiety or phobia in Rac1N mice. Since anxiety was not detected in the exploration tests, the differences observed in wall hugging, floating, and speed might be due to water phobia.

This abnormal behavior may affect the learning performance during the acquisition and reversal phases, as shown by significant increases in the time to reach the platform (genotype effect, $F_{1,22} = 45.11$, $P < 0.0001$), the total distance swum (genotype effect, $F_{1,22} = 4.69$, $P = 0.04$), and the average distance to the goal (genotype effect, $F_{1,22} = 25.66$, $P < 0.0001$) (Fig. 2C–E). Rac1N spatial learning impairment was confirmed by no preference for the trained goal quadrant during the probe trial (genotype effect, $F_{1,22} = 5.45$, $P = 0.02$, Fig. 2F). Finally, these learning deficit were
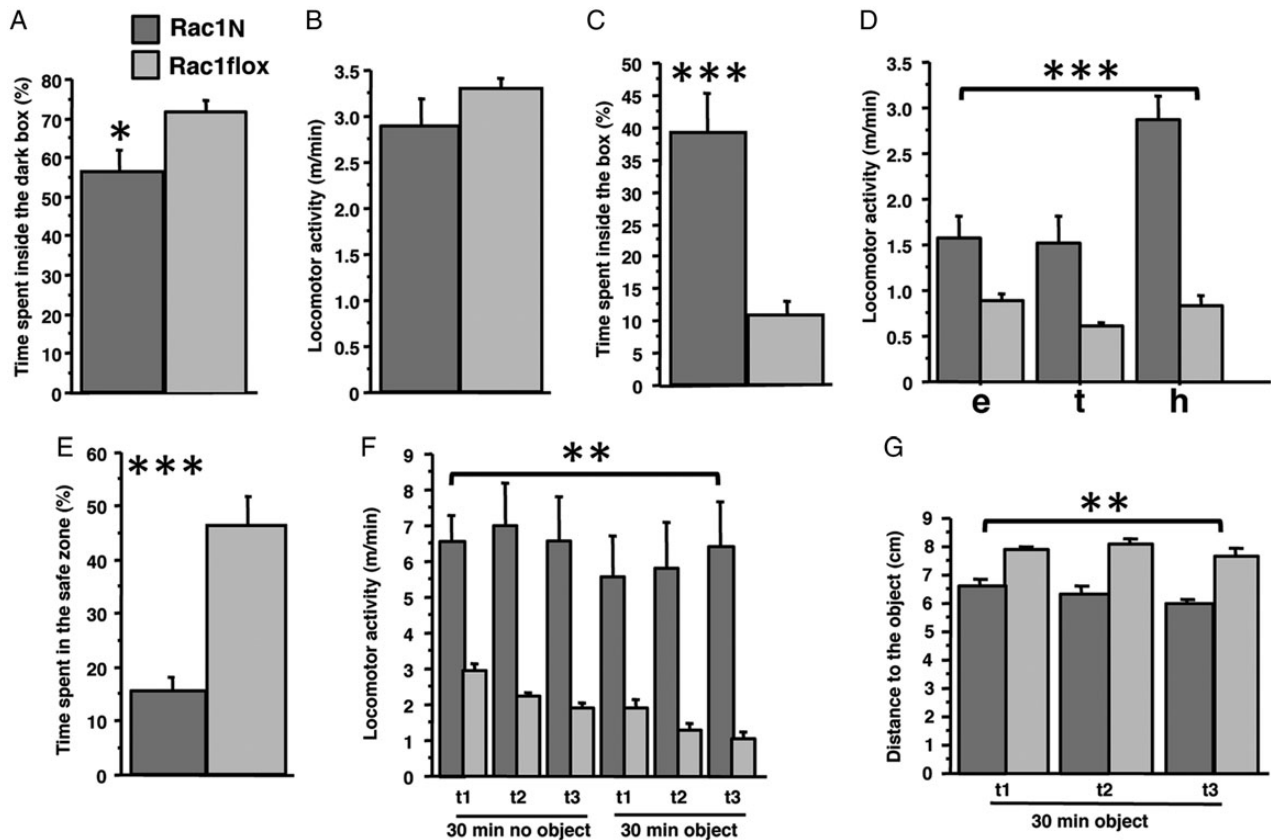
Figure 1. Rac1N mice exhibited hyperactivity but not anxiety-like behavior in the exploration tests. Rac1N ($n = 11$) and Rac1flox ($n = 15$) mice were tested in 3 different explorative tests. In the dark/light box, Rac1N mice spent more time outside the dark box (A) (*$P < 0.05$), and no differences were observed in locomotor activity (B). In the emergence test, the time spent inside the home box (C) and the locomotor activity in all arena zones (D) were significantly higher in the Rac1N mice. In the novelty test, the time spent in the corner (E), the locomotor activity (F), and the distance to the object (G) were significantly different between genotypes. These results indicated that Rac1N mice moved more than control animals. Data are presented as means ± SEM. Zones: e, exploration; h, home; t, transition. **$P < 0.001$; ***$P < 0.0001$.

not caused by defects in visual acuity, since no differences were observed between genotypes in the flag-visible version of the water maze (genotype effect, $F_{1,20} = 0.53$, $P = 0.5$, data not shown).

The data indicate that Rac1N mice are impaired in spatial memory. One possibility is that the observed water phobia may lead to a deficit in attention that would cause a deficit in learning the spatial cues.

Rac1N Mice Hyperactivity Impairs Working Memory

Rac1N and Rac1flox mice were compared with WT and Rac3KO mice in the spontaneous alternation and 8-arm radial maze tasks to comparatively assess working memory performance in the 2 animal models. Intact working memory was observed for the Rac3KO mice: in the spontaneous alternation test, no differences were observed between genotypes for the correct alternations (genotype effect, $F_{1,14} = 0.13$, $P = 0.72$, Fig. 2G) and in the total entries (genotype effect, $F_{1,14} = 0.5$, $P = 0.48$, Fig. 2H). A similar picture was observed in the 8-arms radial maze, where no differences were scored for the correct arm choices (genotype effect, $F_{1,14} = 0.6$, $P = 0.44$, Fig. 2K), number of errors (genotype effect, $F_{1,14} = 0.4$, $P = 0.54$, Fig. 2L), and total number of visits (genotype effect, $F_{1,14} = 1.7$, $P = 0.2$, Fig. 2M). Conversely, Rac1N and Rac1flox mice revealed significant differences in both tests: in spontaneous alternation, Rac1N mice made less correct alternations (genotype effect, $F_{1,21} = 19.9$, $P = 0.0002$, Fig. 2I) as confirmed also by comparing Rac1N mice with Syn-Cre and WT mice (genotype effect on

control mice, $F_{1,36} = 1.14$, $P = 0.3$, Supplementary Fig. 1F). The increased exploration (genotype effect, $F_{1,21} = 12.2$, $P = 0.002$, Fig. 2J) observed in Rac1N mice with respect to Rac1flox mice is possibly influenced by the Syn-Cre transgene, as shown by a significant difference between Rac1flox and Syn-Cre mice (genotype effect, $F_{1,28} = 8.3$, $P = 0.007$, Supplementary Fig. 1G).

In the 8-arm radial maze, while the Rac1flox mice reached a good level of performance, the performance of the Rac1N mice were barely above chance level (genotype effect, $F_{1,13} = 16.4$, $P = 0.001$; Fig. 2N). A borderline difference was observed in the number of total errors, which declined over time in Rac1flox but not in Rac1N mice (genotype effect, $F_{1,13} = 3.2$, $P = 0.09$; Fig. 2O), while a highly significant difference was scored in the total number of visits over the 10 days of training (genotype effect, $F_{1,17} = 54.14$, $P < 0.0001$, Fig. 2P). These results suggest that the hyperactivity observed in these tests may impair the working memory of Rac1N mice.

Associative Memory is Impaired in Rac1N Mice

We then assessed associative learning by subjecting Rac1N and Rac1flox mice as well as Rac3KO and WT mice to the auditory trace fear conditioning. No significant differences were observed between Rac3KO and WT littermates either during the training sessions where the conditioned stimulus (CS: tone) paired with the unconditioned stimulus (US: foot shock) increasingly elicited freezing in both groups (genotype effect, $F_{1,14} = 0.34$, $P = 0.56$, Fig. 3A), or during the 2 testing sessions 24 h later: both Rac3KO
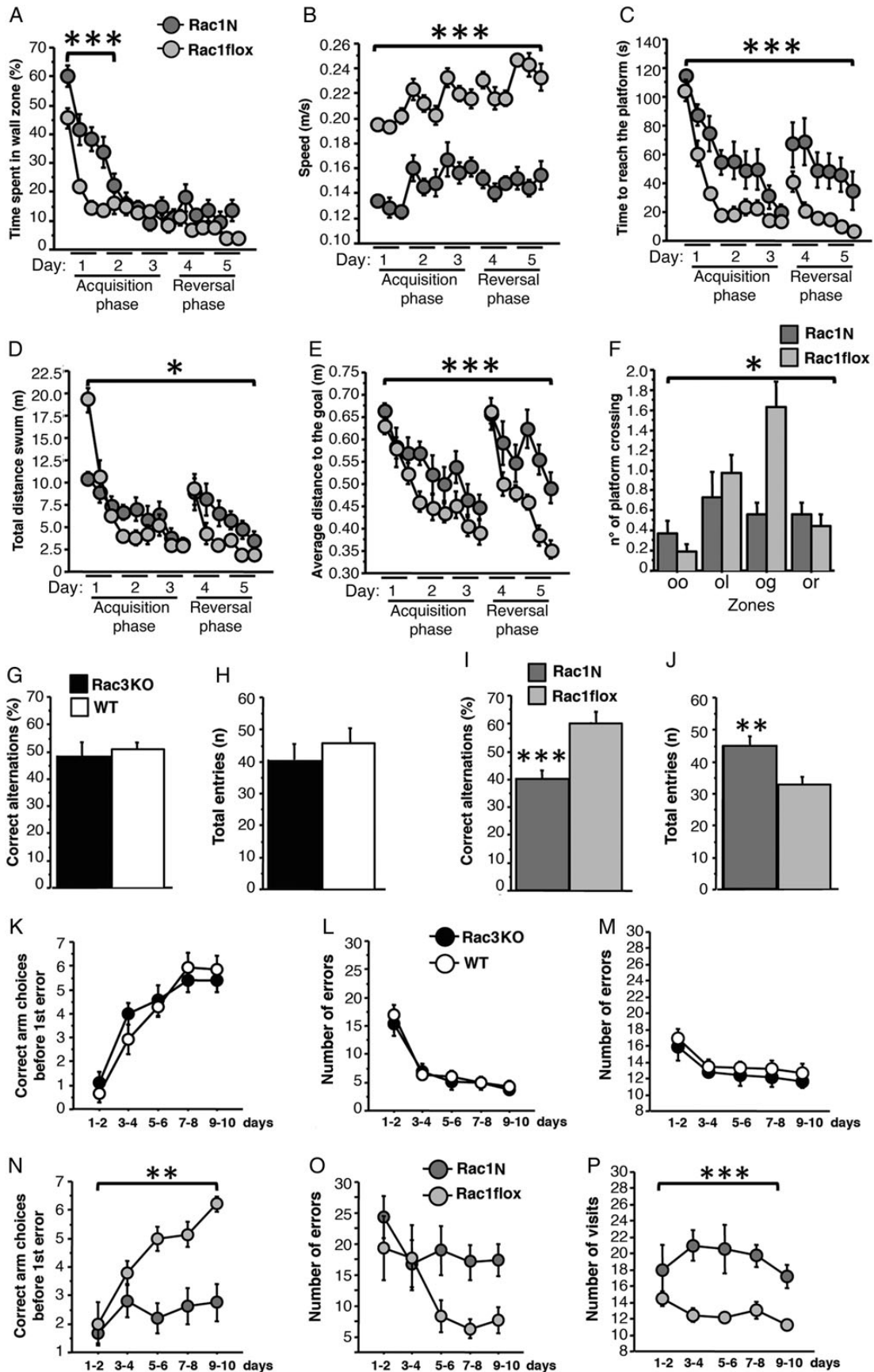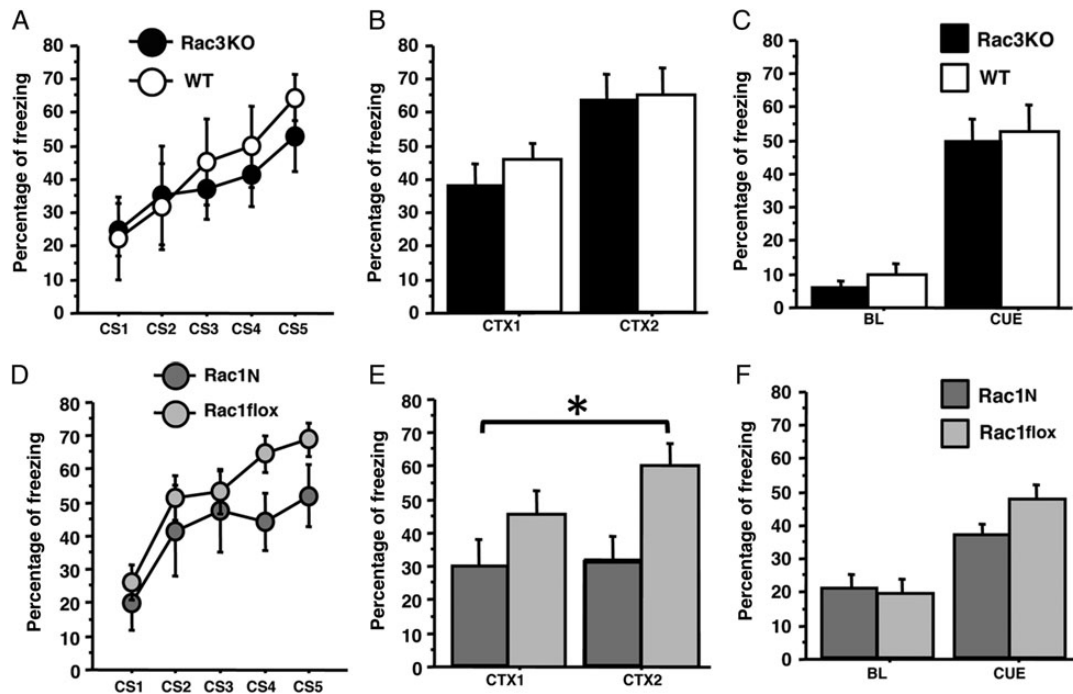
Figure 3. Rac1N but not Rac3KO mice are impaired in associative memory in the trace fear-conditioning. Rac3KO ($n = 8$), WT ($n = 8$), Rac1N ($n = 8$), and Rac1flox ($n = 12$) mice were subjected to the trace fear-conditioning test. Rac3KO mice did not show any difference compared with control mice in freezing reactions during the presentation of the 5 tones (CS) of the conditioning session (A), 24 h later in the 2 min context test (CTX1: first min; CTX2: second min) (B), and during the tone test (BL: baseline; CUE: 1 min tone) (C). Rac1N mice did not show any difference compared with control mice in freezing reactions during the presentation of the 5 tones (CS) of the conditioning session (D), and 24 h later during the tone test (BL: baseline; CUE: 1 min tone) (F). Instead, they showed a specific hippocampal-dependent deficit in the 2 min context test (CTX1: first min; CTX2: second min) (E). Data are presented as means ± SEM. *$P < 0.05$.

and WT remembered the environment when tested for context (genotype effect, $F_{1,14} = 0.25$, $P = 0.62$; Fig. 3B), and when the CS was applied in a new environment (genotype effect, $F_{1,14} = 0.3$, $P = 0.58$, Fig. 3C). Comparison of Rac1N with Rac1flox littermates revealed normal learning during the training session (genotype effect, $F_{1,16} = 2.76$, $P = 0.12$; Fig. 3D), while Rac1N mice showed less freezing during the context test (genotype effect, $F_{1,16} = 5.02$, $P = 0.03$; Fig. 3E). However, Rac1N and Rac1flox equally remembered the CS presented in a new environment (genotype effect, $F_{1,16} = 0.52$, $P = 0.47$, Fig. 3F). These results show that Rac1N mice were able to learn the CS–US, but were specifically impaired in retaining the context memory, suggesting a defect in hippocampal-dependent associative memory.
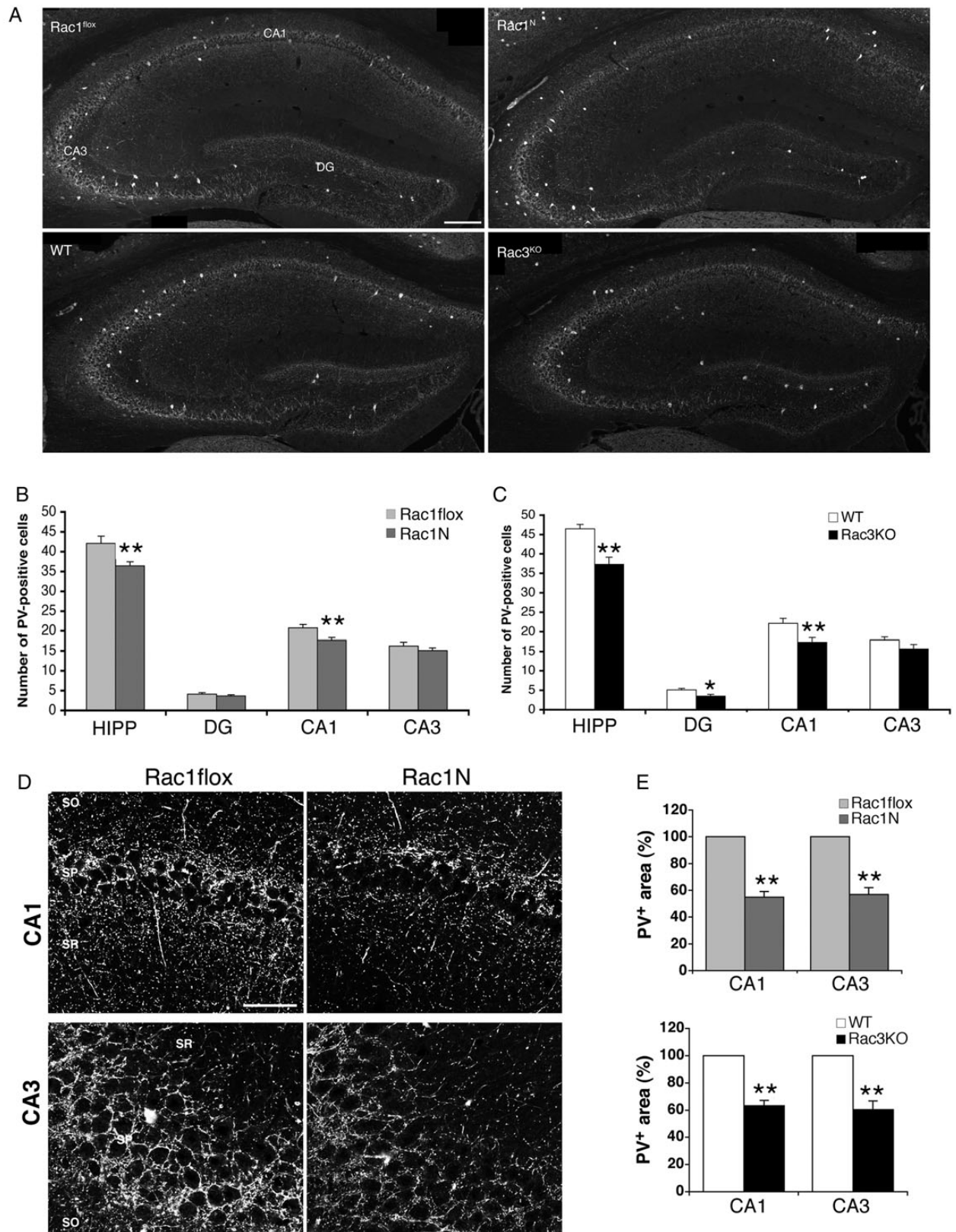
Reduced PV-positive Signal in the Hippocampus of Adult Rac1N and Rac3KO Mice

We have previously shown that Rac3 is expressed and the Syn-Cre transgene is active in developing PV-positive interneurons (Vaghi et al. 2014). Here we have confirmed that the Rac1 protein was decreased by 40% in brain lysates from adult Rac1N compared with Rac1flox mice, and that the SynI-Cre transgene

was active in most adult hippocampal PV-positive cells (Supplementary Fig. 2). Therefore, Rac1 may be deleted in most adult hippocampal PV-positive cells. In addition, we have previously observed a strong and specific loss on PV-positive GABAergic interneurons in the cortex and hippocampus of early postnatal Rac1N/Rac3KO double mutant mice, while other types of cortical and hippocampal GABAergic cells were only weakly affected. In contrast, only a mild reduction of PV-positive cells was observed in the cortex and hippocampus of early postnatal Rac1N or Rac3KO single mutants (Vaghi et al. 2014). Here, we have addressed the role of Rac GTPases on the late development of PV-positive GABAergic cells in the hippocampus of adult mice (Fig. 4A). The decrease in number of PV-positive cells remained limited in the adult single KO mice with respect to their controls: –14% in Rac1N (Fig. 4B) and –20% in Rac3KO hippocampi (Fig. 4C). The reduction of the number of these cells was similar in the CA1 region (–15% and –22% in Rac1N and Rac3KO animals respectively), while no significant decrease in cell number was observed in the CA3 of either KO mice.

The finding that the hippocampi of both Rac1N and Rac3KO animals have less PV-positive cells indicates that the different neurological phenotypes observed in these mice cannot derive just from the limited loss of these interneurons. We postulated

Figure 2. Spatial and working memory analysis on Rac3KO and Rac1[N] mice. Rac1N ($n = 9$) and Rac1flox ($n = 15$) mice were tested for 5 days in the water maze spatial reference memory task. Thigmotaxis (A) and speed (B) are highly different between Rac1N and Rac1flox mice. These differences influence Rac1N mice performance as indicated by the escape latency to locate the new platform (C), the distance swum (D), and the average distance to the goal (E) during the acquisition and reversal phases. In fact, the analysis of the number of platform crossings during the first trial of the reversal phase indicates genotype-dependent differences between mutant and control mice (F) (zones: oo = opposite to old goal; ol = old left; og = old goal; or = old right.). (G–P) Two different sets of mice were tested in the spontaneous alternation ($n = 8$ for Rac3KO and WT mice; $n = 11$ for Rac1N mice; $n = 12$ for Rac1flox mice), and 8-arms radial maze tasks ($n = 8$ for Rac3KO, WT, and Rac1N mice; $n = 12$ for Rac1flox mice). Rac3KO mice did not show working memory defects in either the spontaneous alternation (G,H) or radial maze tasks (K–M). Instead, Rac1N mice are impaired in working memory performance as shown by lower correct alternations in the spontaneous alternation (I), and the lower correct arm choices before the first error (N) and the number of errors (O) in the radial maze. Higher activity was found in the radial maze by the number of visits (P). The increased total entries in the spontaneous alternation (J) are possibly due to the Syn-Cre transgene (see Supplementary Fig. 1G). Data are presented as means ± SEM. *$P < 0.05$; ***$P < 0.001$; ***$P < 0.0001$.

Figure 4. Reduced number of hippocampal PV-positive interneurons in Rac1N and Rac3KO mice. (A) Immunofluorescence to detect PV-positive cells in the hippocampus of single adult KO mice and their respective control littermates (Rac1flox, WT). DG, dentate gyrus. Scale bar: 200 μm. (B,C) Quantification of the number of PV-positive neurons per section of hippocampus from Rac1N, Rac3KO and control littermates. Graph bars are normalized means ± SEM ($n = 25$–40 sections from 3–5 mice/genotype). *$P < 0.05$; **$P < 0.005$. (D) Confocal images of PV staining in the CA1 and CA3 of the hippocampus of mutant (Rac1N) and control (Rac1flox) adult mice. SO, stratum oriens; SP, stratum pyramidale; SR, stratum radiatum. Scale bars, 50 μm. (E) Quantification of the area occupied by the signal for PV in the stratum pyramidale of Rac1N versus Rac1flox, and Rac3KO versus WT littermates, respectively. Bars are normalized means ± SEM of the PV-positive area measured in the SP of hippocampal CA1 and CA3 regions (CA1: $n = 33$–38 fields; CA3: $n = 16$–27 fields; 3–4 mice/genotype). **$P < 0.005$.

a differential effect of the deletion of either Rac on the maturation of the remaining hippocampal PV-positive cells. The main population of hippocampal PV-positive cells is represented by the basket cells that innervate the perisomatic area of the excitatory pyramidal cells. Within the hippocampal CA fields, the PV-positive axon terminals are concentrated in the pyramidal layer (Sik et al. 1995). The signal for PV was markedly reduced in the CA pyramidal layer in both KO lines (Figs. 4D and D): in the CA1 pyramidal layer the PV-positive area was decreased by 45% in Rac1N and by 37% in Rac3KO mice, while in the CA3 region the signal was reduced by 43% and 40% in Rac1N and Rac3KO respectively compared with their control littermates (Fig. 4E). These results show that lack of either Rac1 or Rac3 causes similar defects on the maturation of the PV-positive interneurons, and support the existence of other mechanism(s) responsible for the different functional phenotypes observed in Rac1N and Rac3KO animals.

Differential effects of the depletion of either Rac1 or Rac3 on the maturation of PV-positive interneurons

To test if the depletion of either Rac GTPase affects the synaptic maturation of the PV-positive cells, we looked at the distribution of 2 markers of GABAergic cells: the enzyme glutamic acid decarboxylase (GAD) catalyzes the decarboxylation of glutamate to GABA and marks neuritic processes and synaptic terminals; the vesicular GABA transporter (VGAT) mediates the accumulation of GABA into synaptic vesicles, and is concentrated in the presynaptic axonal endings of GABAergic neurons, thus representing a marker of inhibitory synapses. Different types of GABAergic interneurons may express either one or both GAD65 and GAD67 isoforms. As expected (Fish et al. 2011), the colocalization of PV with GAD65 was limited, while PV colocalized extensively with GAD67 around the soma of pyramidal neurons (data not shown). Quantitative analysis showed that the colocalization in the CA1 pyramidal layer of PV with either VGAT or GAD67 was strongly decreased in both Rac1N and Rac3KO mice compared with their respective controls (Fig. 5A–C). A similar decrease was also detected in the CA3 region (data not shown). Since both GAD67 and VGAT are expected in mature PV-positive terminals, we looked at the colocalization of the 3 markers in the CA1 pyramidal layer of control and KO mice. The area of colocalization of PV, GAD67, and VGAT was significantly decreased in the CA1 pyramidal layer from both Rac1N and Rac3KO with respect to their controls (Fig. 5D, left graph). These data show that the PV-positive signal was significantly affected in the pyramidal layer of both KO animals. Interestingly, the fraction of VGAT-positive area in the CA1 pyramidal layer (=total VGAT-positive area) colocalizing with PV and GAD67 was strongly decreased in Rac1N and only weakly reduced in Rac3KO mice compared with controls (Fig. 5D, right graph). The difference between the reduction observed in Rac1N (–42%) and Rac3KO mice (–11%) was significant (P < 0.001). This result fits with the unexpected finding that the total VGAT-positive area in the CA1 pyramidal layer was significantly decreased in Rac3KO versus WT mice (–25%), but not in Rac1N versus Rac1flox mice (Fig. 5E). Finally, the evaluation of the density of dots positive for both PV and VGAT confirmed that the PV-positive GABAergic presynaptic terminals were significantly decreased in the hippocampal pyramidal layer of Rac1N and Rac3KO mice compared with their respective controls (Fig. 5F).

## Hippocampal Pyramidal Neurons in Rac1N Mice are Hyperexcitable

The reduced development of PV-positive cells and concurrent reduction of PV/VGAT-positive synaptic terminals in the hippocampal

pyramidal layer could affect the functional properties of the hippocampal circuits. We used the whole-cell patch-clamp technique to compare the excitability of pyramidal cells from Rac1N, Rac3KO and control WT, Rac1flox and Syn-Cre mice. We first examined the electrophysiological passive properties of CA1 and CA3 pyramidal neurons, which appeared normal in terms of their number and capacity to form morphological synapses (Supplementary Fig. 3). No differences were detected for membrane capacitance, input resistance, and membrane resting potential between WT, Rac1flox, Syn-Cre, Rac1N, and Rac3KO mice (Table 1). Bath perfusion of brain slices with 500 µM 4-AP induced epileptic-like ictal discharges (Fig. 6A) in 56% of WT, 60% of Rac1flox, and 63% of Syn-Cre hippocampal pyramidal cells examined, and in 82% and 80% of the cells from Rac1N and Rac3KO mice, respectively. Preictal activity was present in all the cells analyzed, including those not showing ictal-like activity, and independently from the genotype. Cells showing ictal-like activity always showed afterdischarges. Despite the time of incubation with 4-AP was similar in all the recorded cells (300 ± 4 s), the interval between the beginning of stimulation with 4-AP and the appearance of the ictal event (TTI, time-to-ictal event) was significantly shorter in Rac1N pyramidal cells (388 ± 29 s) compared with either WT (610 ± 18 s), Rac1flox (593 ± 15 s), or Syn-Cre cells (606 ± 22 s) (Fig. 6B). The ictal events were also significantly longer-lasting in Rac1N than in control cells (duration of ictal-like activity: 53.6 ± 8.5 vs. 22.3 ± 1.8 s) (Fig. 6C). Pyramidal cells from Rac3KO mice had values for TTI (519 ± 25 s) and ictal event duration (31.7 ± 2.7 s) that were intermediate between those measured in control cells (WT, Rac1flox, or Syn-Cre) and Rac1N cells. No significant differences were observed in the amplitude of the ictal events between Rac1N, Rac3KO and control cells (WT, Rac1flox, or Syn-Cre) (Fig. 6D). These data show that Rac1N are more susceptible to 4-AP-elicited epileptiform activity than Rac3KO and WT animals.

These findings may explain the differences between Rac1N and Rac3KO detected by analysis of video-EEG recordings, which revealed epileptic abnormalities (sharp waves) and spontaneous seizures in Rac1N mice during 985 h of recording, with 31 spontaneous seizures detected in 11 out of 18 Rac1N mice (Fig. 6E), the first spontaneous seizure occurring at P29. Neither seizures nor epileptic abnormalities were observed in the Rac3KO, Rac1flox, Syn-Cre, and WT mice during 416, 266, 176, and 125 h of recording, respectively. Therefore, the deletion of Rac1 but not Rac3 induces spontaneous epileptic seizures. Quantitative EEG analysis revealed impaired synchronization of cortical networks in both Rac1N and Rac3KO animals: spectral analysis of background EEG activity showed a significant GROUP effect ($F_{4,79} = 10.573$; $P = 6.52 \times 10^{-7}$) for theta–alpha MDF. At post hoc analysis, Rac1N and Rac3KO mice showed a significantly reduced MDF value compared with WT ($P = 2.06 \times 10^{-5}$ and $P = 0.007$ respectively) and Syn-Cre mice ($P = 0.0002$ and $P = 0.045$ respectively). Compared with Rac1flox mice, Rac1N showed a significant decrease in MDF ($P = 0.0001$), whereas Rac3KO revealed only a trend towards MDF reduction ($P = 0.057$). No significant differences in MDF were found among WT, Syn-Cre and Rac1flox mice, and no significant effects were found for theta–alpha relative power and for both delta band parameters (Supplementary Fig. 4). These results reveal abnormal brain activity in both KO mice, with slower theta–alpha rhythms significantly more evident in Rac1N than in Rac3KO animals.

Hippocampal Pyramidal Neurons in Rac1N Mice Show Reduced sIPSCs

To better analyze the alterations of the synaptic GABAergic inputs, spontaneous inhibitory postsynaptic currents (sIPSCs)
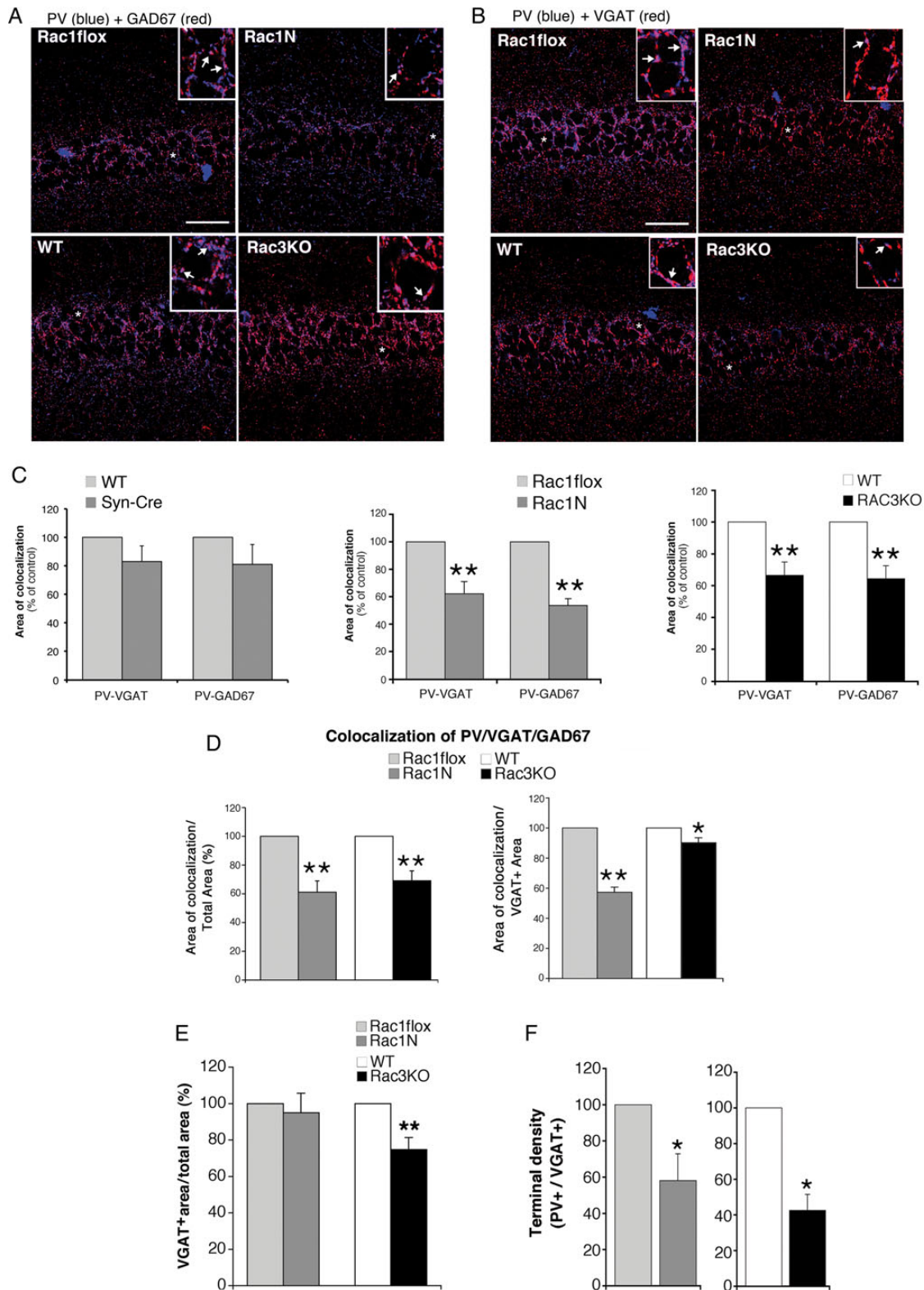
Figure 5. Inhibitory presynaptic input from PV-positive interneurons is reduced in the hippocampus of Rac1N and Rac3KO mice. Confocal images of sections of the CA1 from Rac1flox, Rac1N, WT, and Rac3KO mice costained either for PV and GAD67 (A), or for PV and VGAT (B). Areas of colocalization are in purple. Scale bars, 50 μm. Insets are 3-fold enlargements of the regions marked by asterisks. Arrows indicate areas of colocalization of PV with either GAD67, or VGAT. (C) Quantification of the area of colocalization, normalized to the respective controls (=100%); $n = 19–23$ (Rac1N vs. Rac1flox; Rac3KO vs. WT) and $n = 9–10$ (Syn-Cre vs. WT) CA1 fields per genotype. **$P < 0.005$. (D) Quantification of the area of colocalization of the 3 markers (PV, VGAT, GAD67) within either the corresponding total area of CA1 pyramidal layer (left), or the total VGAT-positive area within the CA1 pyramidal layer (right). Values for Rac1N and Rac3KO samples were normalized to the respective controls (Rac1flox and WT). (E) Quantification of the VGAT-positive area in the CA1 pyramidal layer: graph bars are normalized means ± SEM ($n = 26–30$ CA1 fields from 3 mice/genotype). **$P < 0.005$. (F) Graph bars are normalized means ± SEM of the density of PV/VGAT-positive terminals (number of dots/cell) in the pyramidal layer ($n = 16–20$ fields/genotype). *$P < 0.05$.

Table 1 Passive properties of pyramidal neurons from WT, Rac1N and Rac3KO mice

	C_m (pF)	R_{in} (MΩ)	V_m (mV)
CA3			
Rac1flox ($n = 13$)	127.2 ± 9.6	132.0 ± 17.2	−72.1 ± 3.1
WT ($n = 9$)	122.0 ± 11.5	130.0 ± 16.6	−72.0 ± 3.5
Rac1N ($n = 14$)	123.8 ± 8.0	142.8 ± 8.9	−72.0 ± 1.5
Rac3KO ($n = 11$)	125.4 ± 9.0	127.5 ± 12.7	−70.9 ± 3.2
Syn-Cre ($n = 8$)	118.9 ± 12.3	127.1 ± 11.1	−72.3 ± 3.7
CA1			
Rac1N ($n = 19$)	122.7 ± 7.3	133.1 ± 9.5	−72.9 ± 1.9
Rac3KO ($n = 21$)	123.6 ± 7.5	130.4 ± 7.5	−71.8 ± 1.8
WT ($n = 14$)	121.8 ± 10.0	130.2 ± 12.4	−71.8 ± 2.0
Rac1flox ($n = 19$)	121.4 ± 6.8	131.9 ± 8.2	−71.8 ± 1.7
Syn-Cre ($n = 11$)	119.8 ± 7.7	139.8 ± 12.7	−71.6 ± 1.8

Electrophysiological passive properties were recorded in hippocampal CA pyramidal neurons. Values are means ± SEM. No significant differences were detected. C_m, capacitance; R_{in}, input resistance; V_m, resting potential.

were recorded in the presence of glutamatergic blockers NBQX and CPP in the CA1 glutamatergic pyramidal cells (Fig. 7A). These sIPSCs were abolished by the GABA$_A$ receptor antagonist bicuculline (Fig. 7B), and they were differently affected in Rac1N and Rac3KO neurons. The instantaneous frequency and the amplitude of the sIPSCs were decreased in Rac1N compared with control (WT, Rac1flox, or Syn-Cre) cells, while they were not affected in Rac3KO cells (Fig. 7C,D). On the other hand, the rise and decay times of sIPSCs were similar in control (WT, Rac1flox, or Syn-Cre), Rac3KO and Rac1N mice (Fig. 7E,F).

Altogether, the electrophysiological characterization shows an important difference in the functional consequences of the deletion of either Rac GTPase: while Rac1N mice were more susceptible to the development of ictal-like discharges induced by 4-AP, Rac3KO animals showed an intermediate susceptibility between Rac1N and WT neurons. The difference between the excitability of the 2 Rac mutants was reflected by a clear functional impairment of the inhibitory system in the hippocampus of Rac1N, but not Rac3KO animals. These functional differences may help explaining why only Rac1N mice show spontaneous epileptic activity, and may underlie the behavioral differences between Rac1N and Rac3KO mice.

CB1R-positive terminals are upregulated in Rac1N mice, and may be responsible for the defect in postsynaptic inhibitory currents observed in the pyramidal neurons of Rac1N mice

Intriguingly, comparison of the morphological analysis presented so far with the behavioral, electroencephalographic, and electrophysiological results highlights an apparent contradiction. On one hand the deletion of either GTPase causes a similar loss of PV-positive cells and of PV-positive GABAergic synaptic terminals (Figs 4, 5), with a decrease of total VGAT-positive terminals evident only in the pyramidal layer of Rac3KO animals (Fig. 5E). On the other hand, the behavioral and functional data indicate that only Rac1N mice show cognitive deficits (Figs 1–3), epilepsy (Fig. 6), and the specific functional impairment of the GABAergic system (Fig. 7). We have therefore set to identify other morphological defects that may help explain this apparent contradiction.

We focused the analysis on the synaptic terminals of CCK-positive basket cells that together with the PV-positive basket cells are a distinct major type of GABAergic interneurons targeting the soma and proximal dendrites of the pyramidal neurons in the hippocampus and cortex (Katona et al. 1999; Morozov et al. 2009; Eggan et al. 2010). The presynaptic terminals formed by the CCK-positive interneurons on the pyramidal cells contain high levels of the type 1 cannabinoid receptors (CB1Rs). Interestingly, we observed a strong increase of the CB1R-positive area and of the density of CB1R-positive puncta in the pyramidal layer of Rac1N mice with respect to Rac1flox control mice, while no significant increase was observed in the Rac3KO mice (Fig. 8A–C). These results suggest a specific increase in CB1R-positive presynaptic terminals from CCK-positive cells around pyramidal cell somata of Rac1N mice.

CB1R-positive perisomatic terminals in the CA1 pyramidal layer were largely devoid of GAD67, while they often colocalized with GAD65 (Fig. 8D) as expected, since CCK interneurons mainly express the GAD65 isoform (Wyeth et al 2012; Fish et al 2011). Quantification showed an increase of terminals positive for both CB1R and GAD65 in Rac1N mice compared with Rac1flox, while the increase of the total GAD65-positive terminals was not significant. This may be due to the fact that double-positive terminals represent only 17 and 33% of the total GAD65+ terminals in the pyramidal layer of Rac1flox and Rac1N mice, respectively.

These data suggest that the increase in CB1R-positive terminals observed in the CA1 pyramidal layer of Rac1N mice could compensate for the loss of PV/VGAT-positive terminals observed in these animals, and may explain why the total area of VGAT-positive terminals is decreased in the CA1 pyramidal layer of Rac3KO but not Rac1N mice (Fig. 5E).

Binding of endocannabinoids to CB1Rs selectively inhibits calcium-induced GABA release by the CCK-positive cells, thus preventing inhibition of the principal cells (Wilson and Nicoll 2002). Therefore, it should be possible to revert the decrease in sIPSCs observed in the Rac1N neurons by adding an antagonist for the CB1Rs, to prevent the inhibition of GABA release from CB1R-positive inhibitory terminals (Lee et al. 2010). Accordingly, incubation of brain sections with the CB1R antagonist SR141716A (1 μM) induced an increase in the frequency and amplitude of sIPSCs in both Rac1N and WT CA1 neurons. We measured an increase of 17–19 ± 3–4% in the frequency of sIPSCs in control neurons (from either WT, Rac1flox, or Syn-Cre mice), of +11 ± 2% in Rac3KO neurons, and of +42 ± 9% in Rac1N neurons (Fig. 8E). The increase in frequency induced by the CB1R antagonist measured in Rac1N neurons was significantly larger compared with that observed in WT neurons (Fig. 8F). Moreover, we observed a significant increase in the amplitude of sIPSCs in Rac1N neurons treated with the CB1R antagonist, while no effects were induced by the drug in either Rac3KO, WT, Rac1flox, or Syn-Cre neurons (Fig. 8G,H). The administration of SR141716A did not alter the kinetic of the events in neurons from Rac1N, Rac3KO, Rac1flox, Syn-Cre, or WT mice (Supplementary Fig. 5). Altogether these results indicate that blockade of the CB1Rs by an antagonist partially rescues the defect in sIPSCs observed in Rac1N neurons, possibly by preventing the CB1R-dependent inhibition of GABA release. The data also suggest that the specific increase in CB1R-positive terminals observed in the CA1 of Rac1N mice may contribute to the stronger phenotype observed in these mutants mice compared with Rac3KO mice.

Discussion

We have addressed the role of Rac1 and Rac3 GTPases during GABAergic interneuron development, and shown that single deletion of either Rac has different consequences on the late development of specific populations of hippocampal interneurons. These morphological defects result in the distinct alterations of the hippocampal inhibitory circuits, which are paralleled by
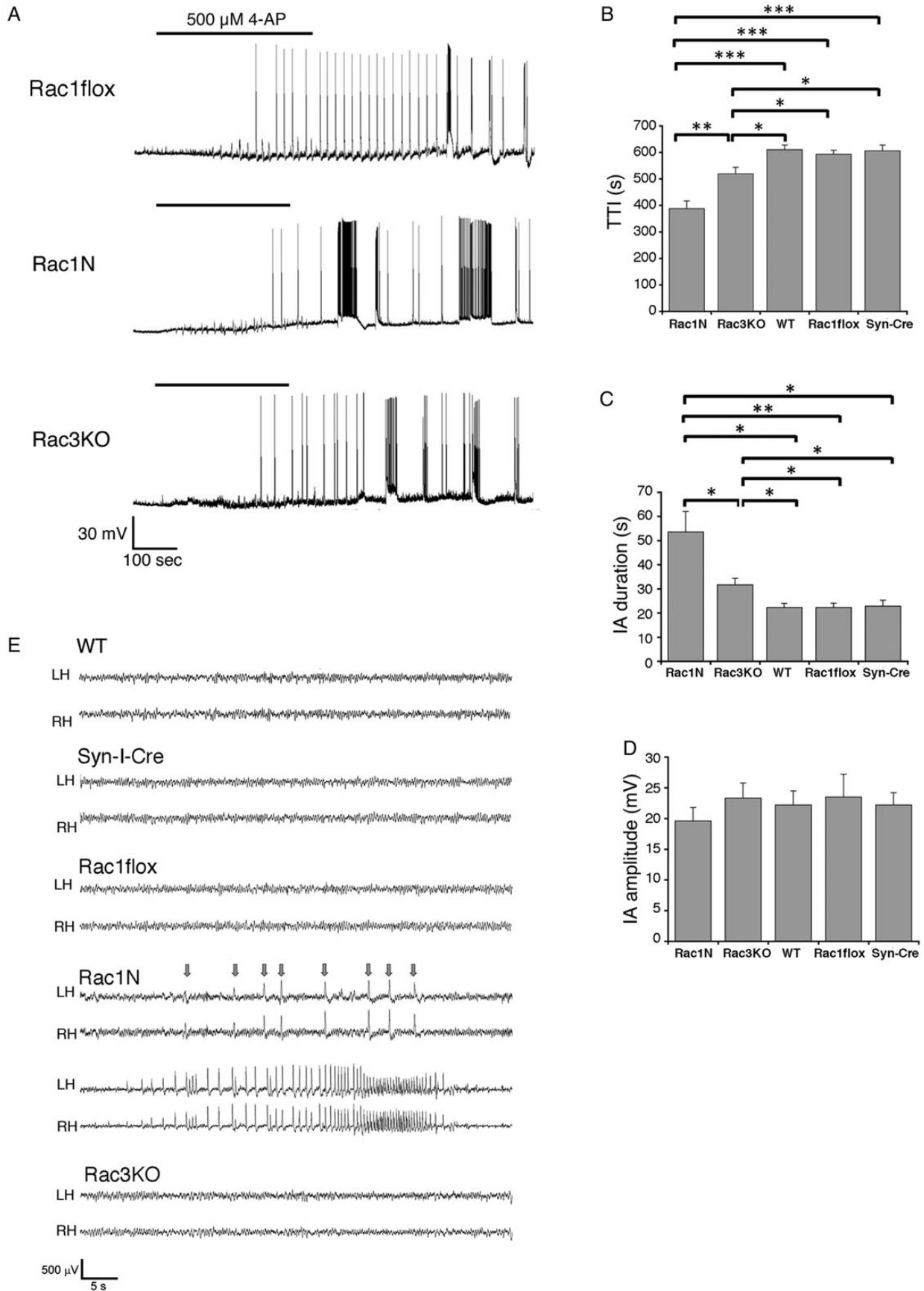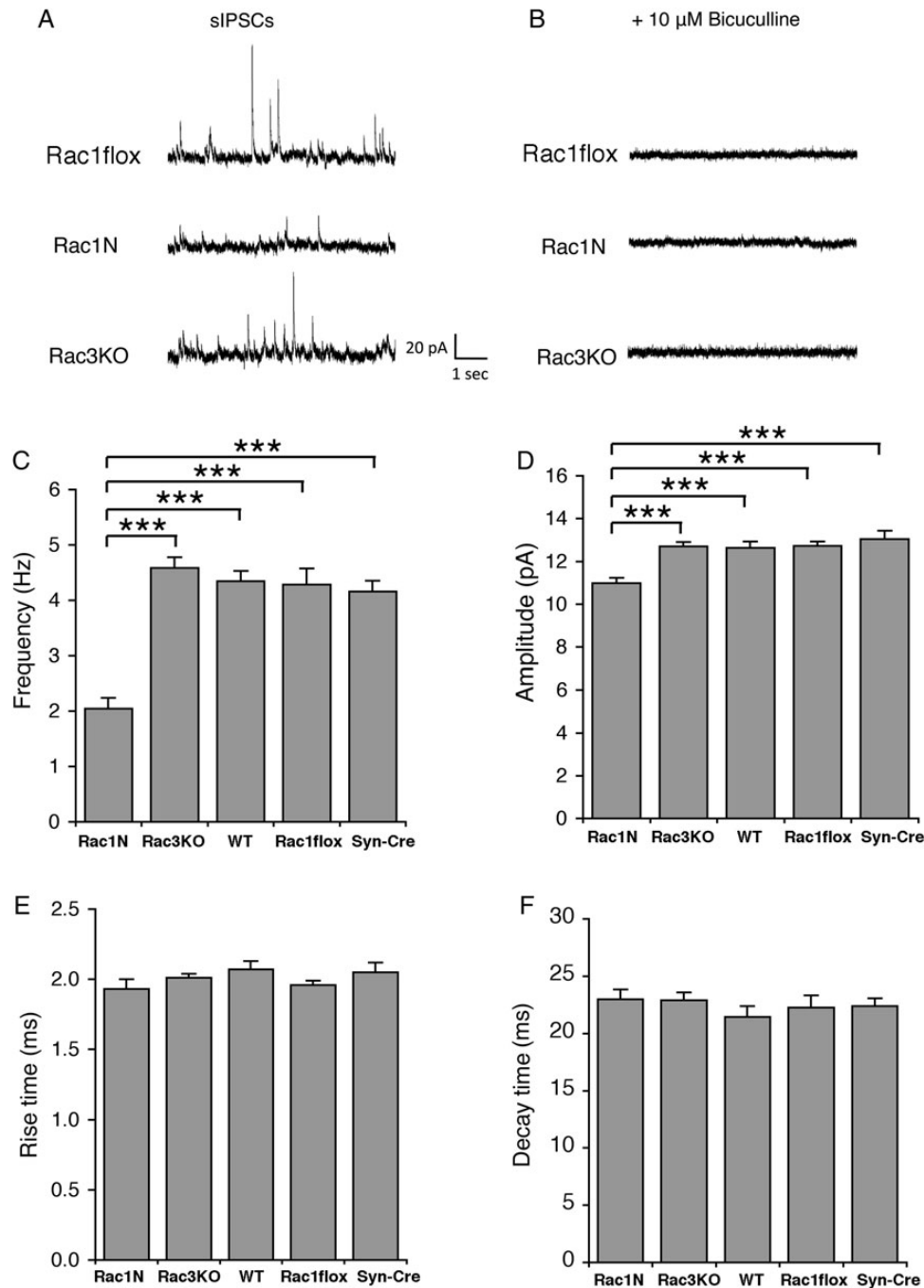
Figure 7. Comparative analysis of spontaneous inhibitory synaptic events in CA1 pyramidal cells. Patch-clamp on brain sections from Rac1flox, Rac1N, and Rac3KO mice was used to record sIPSCs in untreated cells (*A*), and in cells incubated with bicuculline to abolish GABA-dependent IPSCs (*B*). (*C*) Instantaneous frequency of sIPSCs was significantly decreased in Rac1N ($n = 20$) compared with either Rac3KO ($n = 20$), WT ($n = 13$), Rac1flox ($n = 16$), or Syn-Cre ($n = 11$) cells. (*D*) A slight but significant decrease was observed in the amplitude of sIPSCs of Rac1N compared with control (WT, Rac1flox or Syn-Cre) and Rac3KO mice. (*E,F*) Rise and decay time of sIPSCs were similar in control (WT, Rac1flox or Syn-Cre), Rac3KO, and Rac1N neurons. ***$P < 0.001$.

Figure 6. Rac1 or Rac3 deficiency increases hippocampal excitability and susceptibility to 4-AP-elicited epileptiform activity. (*A*) Perfusion with 500 μM 4-AP (continuous black line over each track) induced ictal discharges in 82% Rac1N ($n = 11$), 80% Rac3KO ($n = 10$), and 60% Rac1flox ($n = 10$) CA3 pyramidal neurons. (*B–D*) Quantification of the effects of 500 μM 4-AP on the time-to-ictal event (TTI) (*B*), ictal-like activity (IA) duration (*C*), and amplitude (*D*) ($n = 9$ Rac1N cells; $n = 8$ Rac3KO cells; $n = 5$ WT cells; $n = 6$ Rac1flox cells; $n = 5$ Syn-Cre cells). *$P < 0.05$; **$P < 0.01$; ***$P < 0.001$. (*E*) Electroencephalographic analysis shows spontaneous seizures in Rac1N but not in Rac3KO or control (WT, Syn-Cre, Rac1flox) mice. Examples of raw EEG traces during wakefulness in WT, Syn-Cre, Rac1flox, Rac1N and Rac3KO mice (RH: right hemisphere LH: left hemisphere). Two examples are shown for Rac1N: epileptic sharp waves with larger amplitude than background EEG (arrows in upper traces); spontaneous seizure with continuous spiking activity (bottom traces).
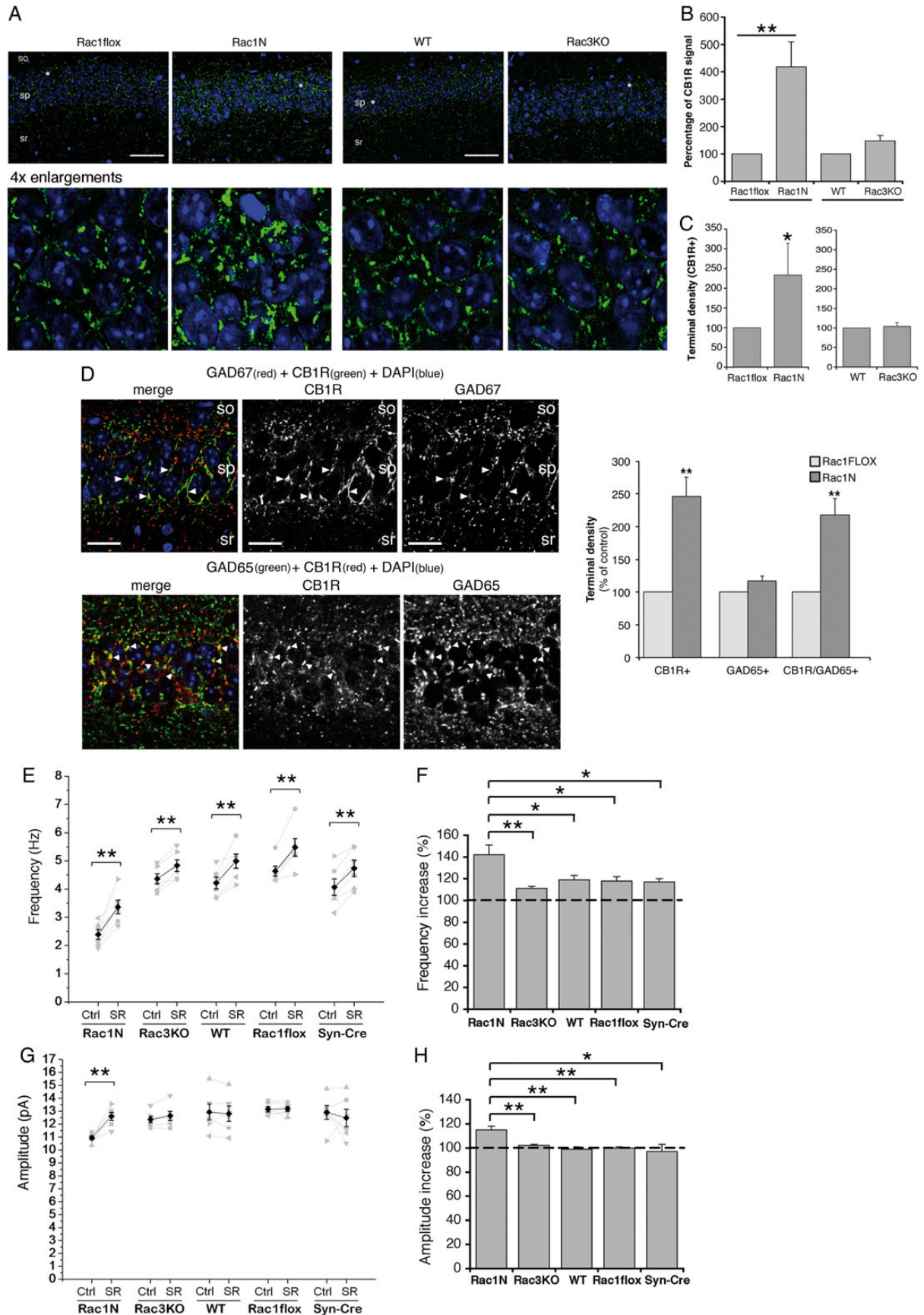
different behavioral and functional phenotypes. Previous studies have established that Rac proteins are important for the development of cortical and hippocampal GABAergic interneurons. In particular, Rac1 is required for the exit from the cell cycle of the MGE-born interneuron precursors (Vidaki et al. 2012), and to confer migratory competence to the differentiating progenitors (Chen et al. 2007). Moreover, recent work by us and others has shown that both GTPases are necessary to regulate the migration of MGE-derived interneurons during late embryogenesis (Vaghi et al. 2014; Tivodar et al. 2015). These studies have also pointed to a possible role of Rac1 and Rac3 proteins in the later development of specific populations of MGE-derived interneurons (Vaghi et al. 2014), and provided evidence for cytoskeletal defects observed in cultured MGE-derived neurons from Rac1/Rac3 double mutant mice that may underlie the observed migratory defects (Tivodar et al. 2015).

The scope of this study has been to exploit the 2 animal models in which the neurally expressed Rac1 or Rac3 proteins have been deleted, to identify the functions of either GTPases in the late development of GABAergic interneurons. Previous full KO of neural-specific Rac3 has shown a behavioral phenotype characterized by hyperactivity (Corbetta et al. 2008), as well as a modest loss of PV-positive interneurons in the early postnatal mice. Here we have extended the analysis to both adult Rac1 and Rac3 KO mice, by including the morphological, behavioral, and functional analysis of the 2 Rac mutants.

With the aim of identifying specific phenotypes for mice defective in either GTPase, we have extended the previous behavioral analysis performed on Rac3KO (Corbetta et al. 2008) to include the Rac1N mice, and we have further expanded the comparative analysis between the 2 genotypes by including a number of other tests aimed at comparing some aspects of their cognitive functions. Tests evaluating the exploratory activity of the mice have shown a greater generalized hyperactive behavior of Rac1N mutants compared with the one previously described in Rac3KO mice. Contrary to previous observations on Rac3KO mice, we found here that Rac1N mutants had evident spatial reference memory defects in the water maze. On the other hand, we cannot exclude that the impairment in spatial learning is a consequence of the water phobia shown by Rac1N mice during this test. More tests revealed additional defects specific for Rac1N mice. Working memory measured by the spontaneous alternation and 8-arm radial maze tests was normal in Rac3KO mice, but clearly affected in Rac1N mice: both tests revealed hyperactivity and reduced performance in these animals. Again, the results indicate that the impairment of working memory in Rac1N mice may be a consequence of their greater hyperactivity. Finally, the comparison of the Rac mutants in the auditory fear-conditioning test revealed a defect only in Rac1N mice: they were able to learn during the training period, but defective in retaining the information, indicating an impairment of their associative

memory. Two main conclusions from the comparative behavioral analysis are that (1) both Rac GTPases are required for the development of normal behavior, (2) but depletion of Rac1 affects behavior more severely by affecting also hippocampus-dependent cognitive functions.

We have recently described the specific reduction of the PV-positive interneurons in the double Rac1/Rac3 KO mice, while other major classes of GABAergic interneurons including somatostatin-, calretinin-, and nNOS-positive cells were only weakly affected (Vaghi et al. 2014). The reduction of PV-positive cells is caused by defects in the migration of their MGE-derived precursors. Here, we have characterized the later maturation of these neurons in the single KO mice that appeared to develop normally up to the second postnatal week. Deletion of either Rac leads to a limited decrease ($\approx$10–15%) of PV-positive neurons in adult mice (Fig. 4A–C). On the other hand, we observed a stronger reduction ($\approx$50%) of the synaptic terminals in the pyramidal layer of Rac1N and Rac3KO mice (Fig. 5). Our interpretation of these data is that the limited loss of PV+ cells in single Rac KO animals may be due to a minor migratory defect originating from the loss of one Rac protein, while the stronger loss of terminals is also due to the effect of either RacKO on the maturation of the remaining PV-positive GABAergic cells. We observed similar reductions of the PV-/VGAT-/GAD-67-positive presynaptic terminals in the CA area of the hippocampus of the 2 mutants. These results indicate that depletion of either Rac has similar negative effects on the late development of the hippocampal PV-positive interneurons that cannot account by themselves for the distinct behavioral phenotypes observed in the 2 mutants.

The comparative EEG and electrophysiological analysis to identify possible defects in the brain and hippocampal circuitry has highlighted other differences between Rac1N and Rac3KO animals. Electrophysiological analysis revealed that the passive properties of CA pyramidal neurons were similar in WT and single KO mice, showing that depletion of either Rac does not alter the intrinsic functional properties of these neurons. On the other hand the CA1 pyramidal cells from Rac1N mice are more sensitive to the action of the convulsant 4-AP, since they could develop earlier and more prolonged ictal-like events compared with either control mice (WT, Rac1flox, or Syn-Cre) or Rac3KO mice that were less sensitive than Rac1N, but more prone than control animals to develop ictal-like events (Fig. 6).

Quantitative EEG on freely moving mice revealed abnormal brain activity in both Rac KO mice, with more evident significant slowing of theta–alpha rhythms in Rac1N than in Rac3KO animals (Supplementary Fig. 4). Since Rac1N but not Rac3KO have seizures, the observed slowing of background oscillatory activity in these 2 groups cannot be fully explained as a mere consequence of repeated epileptic discharges, but is rather consistent with the observed histological and electrophysiological hippocampal abnormalities, being this structure the main source of theta brain rhythms (Buzsáki 2002).

Figure 8. The increased density of CB1R-positive terminals may contribute to the reduced postsynaptic inhibitory currents observed in the CA1 pyramidal neurons of Rac1N mice. (A) Confocal images of the CA1 region from adult mice immunostained for CB1R. CB1R-immunoreactive axon terminals were mainly found around the soma of the pyramidal cells of control mice, and their density was increased in Rac1N mice. No differences were observed between WT and Rac3KO mice (so, stratum oriens; sp, stratum pyramidale; sr, stratum radiatum). Scale bars, 50 μm. Each image of the bottom row is a 4-fold enlargement of part of the pyramidal layer (asterisks) shown in the respective top row image. (B) Graph bars are normalized means ± SEM of the area of the pyramidal layer positive for CB1R (WT = 100%; n = 18 CA1 fields for Rac1N and Rac1flox littermates; n = 19 CA1 fields for Rac3KO and WT littermates; 3 mice/genotype). **P < 0.005. (C) Graph bars are normalized means ± SEM of the density of CB1R-positive terminals (number of dots/cell) in the pyramidal layer (n = 14–18 fields/genotype). * P < 0.05. (D) Upper panels: GAD67 (red) is poorly expressed by the CB1R-positive terminals (green) in the CA1 of Rac1N mice. Arrowheads point to CB1R-positive puncta with low/no signal for GAD67. Lower panels: several CB1R-positive terminals colocalized with GAD65 (arrowheads). Scale bars, 20 μm. Quantifications are shown in the graph on the right (n = 47–49 fields from 16 hippocampal sections/genotype). (E–H) Changes in the frequency (E,F) and amplitude (G,H) of sIPSCs recorded in mutant (Rac1N, Rac3KO) and control (WT, Rac1flox, Syn-Cre) CA1 pyramidal neurons before (Ctrl) and after (SR) incubation with the CB1R antagonist SR141716A (n = 6 cells per genotype). (E,G) Each gray line represents the measurements from a single neuron; black lines are mean values. (F,H) Graph bars show the changes in frequency (F) and amplitude (H) of sIPSCs expressed as percentages of controls. *P < 0.05; **P < 0.01.

Taken together, the electrophysiological and EEG data demonstrate a stronger hyperexcitability of Rac1N mice. The hypothesis that this stronger hyperexcitability was due to an altered balance between excitatory and inhibitory inputs on pyramidal cells was supported by the finding that spontaneous GABAergic IPSCs were reduced in the CA1 of Rac1N mice compared with control (WT, Rac1flox, Syn-Cre) and Rac3KO mice, probably due to a reduction in spontaneous firing from GABergic interneurons (Fig. 7). Again, the similar reduction of PV-positive synaptic contacts observed in the CA1 of either mutant is not sufficient to explain the noticeable differences observed in the excitability of their pyramidal cells.

Two main types of interneurons target the soma of hippocampal pyramidal cells to control their activity: the MGE-derived PV-positive basket cells and the CCK-positive basket cells deriving from the caudal GE and characterized by synaptic terminals positive for CB1R (Morozov et al. 2009). PV-positive basket cells form the majority of presynaptic GABAergic contacts on the pyramidal cells of hippocampal CA1/CA3. Therefore the important loss of PV-positive presynaptic terminals observed in the CA1 of Rac mutants should cause a decrease of the total VGAT-positive terminals in the pyramidal layer. While VGAT was significantly decreased in the CA1 of Rac3KO mice, to our surprise it was not reduced in Rac1N mice (Fig. 5E). On the other hand, we detected a striking increase in CB1R-positive terminals only in the CA1 of Rac1N, which may account for the higher concentration of VGAT-positive terminals in the pyramidal layer of these mice.

The CB1R-/CCK-positive basket cells modulate the excitability of both hippocampal pyramidal and PV-positive basket cells by making GABAergic synaptic contacts with both neuronal types (Karson et al. 2009). In turn CCK-positive cells are modulated by cannabinoids: activated pyramidal cells release cannabinoids that activate the CB1R on the terminals of CCK-positive basket cells, thereby inhibiting the release of GABA specifically on the active pyramidal neurons: a form of short-term plasticity known as depolarization-induced suppression of inhibition (Katona et al. 1999; Katona et al. 2001; Ohno-Shosaku et al. 2001; Wilson et al. 2001). The upregulation of CB1R-positive terminals in the CA1 of Rac1N mice may underlie the different behavioral and electrophysiological phenotypes observed in these animals.

We speculate that 2 mechanisms may contribute to the increased excitability observed in the Rac1N pyramidal cells. First, the observed increase in CB1R may increase the cannabinoid-mediated inhibition of GABA release on pyramidal cells, thus increasing their excitability. In this view, CB1R represents a target to attempt the partial rescue of the drastic decrease of the frequency of sIPSCs in Rac1N pyramidal cells. In support of this hypothesis, we have shown that incubation with a CB1R antagonist that prevents the cannabinoid-induced inhibition of GABA release from CCK-positive cells (Katona et al. 1999) is able to increase the frequency of the sIPSCs both in Rac1N and in WT CA1 pyramidal cells; and the effect was more conspicuous in the Rac1N cells, suggesting that preventing the inhibition of GABA release by the CB1Rs can partially rescue the defect in the Rac1N animals (Fig. 8). Second, we hypothesize that in Rac1N mice the increase of the CB1R-positive terminals by CCK cells on pyramidal neurons may be accompanied by an increase of CB1R-negative terminals made by the same population of CCK-positive cells onto PV-positive interneurons (Karson et al. 2009). This is expected to reduce the excitability of the PV-positive cells, and therefore it may at least in part be responsible for the observed decrease in the frequency and amplitude of sIPSCs observed in CA1 Rac1N pyramidal cells (Fig. 7).

It has been proposed that CCK- and PV-positive cells play distinct roles to coordinately modulate the outcome of hippocampal pyramidal cells, by contributing differently to network oscillations: given their firing time and their sensitivity to endocannabinoids, CCK-positive cells may aid in differentiating subgroups of pyramidal neurons, whereas PV-positive cells would synchronize the entire network (Klausberger et al. 2005). The reduction of GABA release from the CB1R-positive terminals in the CA region of the hippocampus is the proposed mechanism by which CB1R ligands may influence the oscillations of the hippocampal network and the associated cognitive functions. In this respect, CB1R activation appears to impair memory formation and consolidation (Clarke et al. 2008; Puighermanal et al. 2009; Wise et al. 2009). Therefore, we suggest that the increase in CB1R-positive terminals observed in the Rac1N mice may at least in part explain the negative effects observed on different forms of memory in these mutants.

In this study, we have identified distinct alterations of specific inhibitory components upon deletion of either Rac1 or Rac3, which result in different alteration of neuronal excitability and behavior. The effects are more pronounced in the Rac1N mutants, where morphological alterations of the inhibitory circuitry are more evident.

Rac GTPases act by interacting with specific effectors to trigger specific signaling pathways. The information about effectors or pathways specifically triggered by either one of the 2 Rac proteins analyzed in this study is very limited. Rac3 has been shown to have some specific effects in different cell lines. For example, knockdown of Rac3, but not of Rac1, results in the induction of autophagy in different cell lines (Zhu et al 2011). Moreover, it has been reported that Rac1 and Rac3 have opposite effects on the adhesion of N1E-115 neuroblastoma cells (Hajdo-Milasinović et al. 2007). In contrast to Rac1, Rac3 inhibits differentiation of neuroblastoma cells by interacting differently with GIT1/βPIX, a protein complex involved in the regulation of cell adhesion and motility (Hajdo-Milasinović et al. 2009). We have not been able to find biochemical differences in the interaction of Rac1 and Rac3 with the GIT complexes isolated from the embryonic brain (Di Cesare et al. 2000). On the other hand, we have been able to observe specific positive effects of the avian ortholog of Rac3 over-expression on the branching of cultured primary retinal neurons (Albertinazzi et al 1998). Based on these observations, it will be interesting to investigate the role of these proteins in the Rac-dependent maturation of interneurons, by exploiting the possibility of analyzing their development in vitro. Interestingly, it has been recently shown that GIT1 deficiency in mice causes attention deficit hyperactivity disorder-like phenotypes, as well as reduced inhibitory presynaptic input and PV-positive signal in the hippocampal CA1 (Won et al 2011), as observed in the Rac KO mice described here.

Several questions remain to be addressed to fully understand the role of each Rac on the different interneurons analyzed in this study. The alteration of the development of CB1R-positive CCK- and of PV-positive cells has been implicated in neurological and psychiatric disorders, and suggested to underlie the cortical oscillation deficits and working memory impairments observed in neural disorders such as schizophrenia (Curley and Lewis 2012). Interestingly, CB1Rs are present also on the hippocampal glutamatergic terminals of principal cells, where they have been shown to provide endogenous protection against kainate-induced epileptic seizures (Monory et al. 2006). Therefore, any further insights in the role of Rac GTPases and associated intracellular mechanisms in the late maturation of CCK- and PV-positive interneurons, as well as in the endocannabinoid-mediated

control of hippocampal glutamatergic neurotransmission will be important to the understanding of the pathogenesis of disorders associated with the alteration of the excitatory neuronal activity.

Supplementary material

Supplementary Material can be found at http://www.cercor.oxfordjournals.org/ online.

Funding

Notes

References

Albertinazzi C, Gilardelli D, Paris S, Longhi R, de Curtis I. 1998. Overexpression of a neural-specific rho family GTPase, cRac1B, selectively induces enhanced neuritogenesis and neurite branching in primary neurons. J Cell Biol. 142:815–825.

Batista-Brito R, Fishell G. 2009. The developmental integration of cortical interneurons into a functional network. Curr Top Dev Biol. 87:81–118.

Bolis A, Corbetta S, Cioce A, de Curtis I. 2003. Differential distribution of Rac1 and Rac3 GTPases in the developing mouse brain: implications for a role of Rac3 in Purkinje cell differentiation. Eur J Neurosci. 18:2417–2424.

Brooks-Kayal A. 2011. Molecular mechanisms of cognitive and behavioral comorbidities of epilepsy in children. Epilepsia. 52(Suppl 1):13–20.

Buzsáki G. 2002. Theta oscillations in the hippocampus. Neuron. 33:325–340.

Cambiaghi M, Cursi M, Monzani E, Benfenati F, Comi G, Minicucci F, Valtorta F, Leocani L. 2013. Temporal evolution of neurophysiological and behavioral features of synapsin I/II/III triple knock-out mice. Epilepsy Res. 103:153–160.

Chen L, Liao G, Waclaw RR, Burns KA, Linquist D, Campbell K, Zheng Y, Kuan CY. 2007. Rac1 controls the formation of midline commissures and the competency of tangential migration in ventral telencephalic neurons. J Neurosci. 27:3884–3893.

Clarke JR, Rossato JI, Monteiro S, Bevilaqua LR, Izquierdo I, Cammarota M. 2008. Posttraining activation of CB1 cannabinoid receptors in the CA1 region of the dorsal hippocampus impairs object recognition long-term memory. Neurobiol Learn Mem. 90:374–378.

Corbetta S, D'Adamo P, Gualdoni S, Braschi C, Berardi N, de Curtis I. 2008. Hyperactivity and novelty-induced hyperreactivity in mice lacking Rac3. Behav Brain Res. 186:246–255.

Corbetta S, Gualdoni S, Albertinazzi C, Paris S, Croci L, Consalez GG, de Curtis I. 2005. Generation and characterization of Rac3 knockout mice. Mol Cell Biol. 25:5763–5776.

Corbetta S, Gualdoni S, Ciceri G, Monari M, Zuccaro E, Tybulewicz VL, de Curtis I. 2009. Essential role of Rac1 and Rac3 GTPases in neuronal development. FASEB J. 23:1347–1357.

Curley AA, Lewis DA. 2012. Cortical basket cell dysfunction in schizophrenia. J Physiol. 590:715–724.

D'Adamo P, Masetti M, Bianchi V, Morè L, Mignogna ML, Giannandrea M, Gatti S. 2014. RAB GTPases and RAB-interacting proteins and their role in the control of cognitive functions. Neurosci Biobehav Rev. 46:302–314.

D'Adamo P, Welzl H, Papadimitriou S, Raffaele di Barletta M, Tiveron C, Tatangelo L, Pozzi L, Chapman PF, Knevett SG, Ramsay MF, et al. 2002. Deletion of the mental retardation gene Gdi1 impairs associative memory and alters social behavior in mice. Hum Mol Genet. 11:2567–2580.

de Curtis I. 2008. Functions of Rac GTPases during neuronal development. Dev Neurosci. 30:47–58.

Di Cesare A, Paris S, Albertinazzi C, Dariozzi S, Andersen J, Mann M, Longhi R, de Curtis I. 2000. p95-APP1 links membrane transport to Rac-mediated reorganization of actin. Nat Cell Biol. 2:521–530.

Eggan SM, Melchitzky DS, Sesack SR, Fish KN, Lewis DA. 2010. Relationship of cannabinoid CB1 receptor and cholecystokinin immunoreactivity in monkey dorsolateral prefrontal cortex. Neuroscience. 169:1651–1661.

Fish KN, Sweet RA, Lewis DA. 2011. Differential distribution of proteins regulating GABA synthesis and reuptake in axon boutons of subpopulations of cortical interneurons. Cereb Cortex. 21:2450–2460.

Gelman DM, Marín O. 2010. Generation of interneuron diversity in the mouse cerebral cortex. Eur J Neurosci. 31:2136–2141.

Hajdo-Milasinović A, Ellenbroek SI, van Es S, van der Vaart B, Collard JG. 2007. Rac1 and Rac3 have opposing functions in cell adhesion and differentiation of neuronal cells. J Cell Sci. 120:555–566.

Hajdo-Milasinović A, van der Kammen RA, Moneva Z, Collard JG. 2009. Rac3 inhibits adhesion and differentiation of neuronal cells by modifying GIT1 downstream signaling. J Cell Sci. 122:2127–2136.

Hernández-Miranda LR, Parnavelas JG, Chiara F. 2010. Molecules and mechanisms involved in the generation and migration of cortical interneurons. ASN Neuro. 2:e00031.

Inan M, Welagen J, Anderson SA. 2012. Spatial and temporal bias in the mitotic origins of somatostatin- and parvalbumin-expressing interneuron subgroups and the chandelier subtype in the medial ganglionic eminence. Cereb Cortex. 22:820–827.

Karson MA, Tang AH, Milner TA, Alger BE. 2009. Synaptic cross talk between perisomatic-targeting interneuron classes expressing cholecystokinin and parvalbumin in hippocampus. J Neurosci. 29:4140–4154.

Katona I, Rancz EA, Acsady L, Ledent C, Mackie K, Hajos N, Freund TF. 2001. Distribution of CB1 cannabinoid receptors in the amygdala and their role in the control of GABAergic transmission. J Neurosci. 21:9506–9518.

Katona I, Sperlagh B, Sik A, Kafalvi A, Vizi ES, Mackie K, Freund TF. 1999. Presynaptically located CB1 cannabinoid receptors regulate GABA release from axon terminals of specific hippocampal interneurons. J Neurosci. 19:4544–4558.

Klausberger T, Marton LF, O'Neill J, Huck JH, Dalezios Y, Fuentealba P, Suen WY, Papp E, Kaneko T, Watanabe M, et al. 2005. Complementary roles of cholecystokinin- and parvalbumin-expressing GABAergic neurons in hippocampal network oscillations. J Neurosci. 25:9782–9793.

Lee SH, Földy C, Soltesz I. 2010. Distinct endocannabinoid control of GABA release at perisomatic and dendritic synapses in the hippocampus. J Neurosci. 30:7993–8000.

Madani R, Kozlov S, Akhmedov A, Cinelli P, Kinter J, Lipp HP, Sonderegger P, Wolfer DP. 2003. Impaired explorative behavior

and neophobia in genetically modified mice lacking or overexpressing the extracellular serine protease inhibitor neuroserpin. Mol Cell Neurosci. 23:473–494.

Malosio ML, Gilardelli D, Paris S, Albertinazzi C, de Curtis I. 1997. Differential expression of distinct members of Rho family GTP-binding proteins during neuronal development: identification of Rac1B, a new neural-specific member of the family. J Neurosci. 17:6717–6728.

Monory K, Massa F, Egertová M, Eder M, Blaudzun H, Westenbroek R, Kelsch W, Jacob W, Marsch R, Ekker M, et al. 2006. The endocannabinoid system controls key epileptogenic circuits in the hippocampus. Neuron. 51:455–466.

Morozov YM, Ayoub AE, Rakic P. 2006. Translocation of synaptically connected interneurons across the dentate gyrus of the early postnatal rat hippocampus. J Neurosci. 26:5017–5027.

Morozov YM, Torii M, Rakic P. 2009. Origin, early commitment, migratory routes, and destination of cannabinoid type 1 receptor-containing interneurons. Cereb Cortex. 19:i78-i89.

Ohno-Shosaku T, Maejima T, Kano M. 2001. Endogenous cannabinoids mediate retrograde signals from depolarized postsynaptic neurons to presynaptic terminals. Neuron. 29:729–738.

Puighermanal E, Marsicano G, Busquets-Garcia A, Lutz B, Maldonado R, Ozaita A. 2009. Cannabinoid modulation of hippocampal long-term memory is mediated by mTOR signaling. Nat Neurosci. 12:1152–1158.

Sik A, Penttonen M, Ylinen A, Buzsáki G. 1995. From Hippocampal CA1 interneurons: an in vivo intracellular labeling study. J Neurosci. 15:6651–6665.

Soriano P. 1999. Generalized lacZ expression with the ROSA26 Cre reporter strain. Nat Genet. 21:70–71.

Stoop R, Pralong E. 2000. Functional connections and epileptic spread between hippocampus, entorhinal cortex and amygdala in a modified horizontal slice preparation of the rat brain. Eur J Neurosci. 12:3651–3663.

Tivodar S, Kalemaki K, Kounoupa Z, Vidaki M, Theodorakis K, Denaxa M, Kessaris N, de Curtis I, Pachnis V, Karagogeos D. 2015. Rac-GTPases regulate microtubule stability and axon growth of cortical GABAergic interneurons. Cereb Cortex. 25:2370–2382.

Tricoire L, Pelkey KA, Erkkila BE, Jeffries BW, Yuan X, McBain CJ. 2011. A blueprint for the spatiotemporal origins of mouse hippocampal interneuron diversity. J Neurosci. 31:10948–10970.

Vaghi V, Pennucci R, Talpo F, Corbetta S, Montinaro V, Barone C, Croci L, Spaiardi P, Consalez GG, Biella G, et al. 2014. Rac1 and rac3 GTPases control synergistically the development of cortical and hippocampal GABAergic interneurons. Cereb Cortex. 24:1247–1258.

Vidaki M, Tivodar S, Doulgeraki K, Tybulewicz V, Kessaris N, Pachnis V, Karagogeos D. 2012. Rac1-dependent cell cycle exit of MGE precursors and GABAergic interneuron migration to the cortex. Cereb Cortex. 22:680–692.

Walmsley MJ, Ooi SK, Reynolds LF, Smith SH, Ruf S, Mathiot A, Vanes L, Williams DA, Cancro MP, Tybulewicz VL. 2003. Critical roles for Rac1 and Rac2 GTPases in B cell development and signaling. Science. 302:459–462.

Welch PD. 1967. The use of fast Fourier transform for the estimation of power spectra: a method based on time averaging over short, modified periodograms. IEEE Trans Audio Electroacoustics. 15:70–73.

Wilson RI, Kunos G, Nicoll RA. 2001. Presynaptic specificity of endocannabinoid signaling in the hippocampus. Neuron. 31:453–462.

Wise LE, Thorpe AJ, Lichtman AH. 2009. Hippocampal CB(1) receptors mediate the memory impairing effects of Delta (9)-tetrahydrocannabinol. Neuropsychopharmacology. 34:2072–2080.

Wolfer DP, Lipp HP. 1992. A new computer program for detailed off-line analysis of swimming navigation in the Morris water maze. J Neurosci Methods. 41:65–74.

Won H, Mah W, Kim E, Kim JW, Hahm EK, Kim MH, Cho S, Kim J, Jang H, Cho SC, et al. 2011. GIT1 is associated with ADHD in humans and ADHD-like behaviors in mice. Nat Med. 17:566–572.

Wonders CP, Anderson SA. 2006. The origin and specification of cortical interneurons. Nat Rev Neurosci. 7:687–696.

Wyeth MS, Zhang N, Houser CR. 2012. Increased cholecystokinin labeling in the hippocampus of a mouse model of epilepsy maps to spines and glutamatergic terminals. Neuroscience. 202:371–383.

Zhu Y, Romero MI, Ghosh P, Ye Z, Charnay P, Rushing EJ, Marth JD, Parada LF. 2001. Ablation of NF1 function in neurons induces abnormal development of cerebral cortex and reactive gliosis in the brain. Genes Dev. 15:859–876.

Zhu WL, Hossain MS, Guo DY, Liu S, Tong H, Khakpoor A, Casey PJ, Wang M. 2011. A role for Rac3 GTPase in the regulation of autophagy. J Biol Chem. 286:35291–35298.